JOURNAL OF GEOPHYSICAL RESEARCH, VOL. 113, G01025, doi:10.1029/2007JG000562, 2008

Use of FLUXNET in the Community Land Model development

R. Stöckli,[1,2,3] D. M. Lawrence,[4] G.-Y. Niu,[5] K. W. Oleson,[4] P. E. Thornton,[4] Z.-L. Yang,[5] G. B. Bonan,[4] A. S. Denning,[1] and S. W. Running[6]

Received 26 July 2007; revised 12 October 2007; accepted 21 December 2007; published 19 March 2008.

[1] The Community Land Model version 3 (CLM3.0) simulates land-atmosphere exchanges in response to climatic forcings. CLM3.0 has known biases in the surface energy partitioning as a result of deficiencies in its hydrological and biophysical parameterizations. Such models, however, need to be robust for multidecadal global climate simulations. FLUXNET now provides an extensive data source of carbon, water and energy exchanges for investigating land processes, and it encompasses a global range of ecosystem-climate interactions. Data from 15 FLUXNET sites are used to identify and improve model deficiencies. Including a prognostic aquifer, a bare soil evaporation resistance formulation and numerous other changes in the model result in a significantly improved soil hydrology and energy partitioning. Terrestrial water storage increased by up to 300 mm in warm climates and decreased in cold climates. Nitrogen control of photosynthesis is revealed as another missing process in the model. These improvements increase the correlation coefficient of hourly and monthly latent heat fluxes from a range of 0.5–0.6 to the range of 0.7–0.9. RMSE of the simulated sensible heat fluxes decrease by 20–50%. Primary production is overestimated during the wet season in mediterranean and tropical ecosystems. This might be related to missing carbon-nitrogen dynamics as well as to site-specific parameters. The new model (CLM3.5) with an improved terrestrial water cycle should lead to more realistic land-atmosphere exchanges in coupled simulations. FLUXNET is found to be a valuable tool to develop and validate land surface models prior to their application in computationally expensive global simulations.

Citation: Stöckli, R., D. M. Lawrence, G.-Y. Niu, K. W. Oleson, P. E. Thornton, Z.-L. Yang, G. B. Bonan, A. S. Denning, and S. W. Running (2008), Use of FLUXNET in the Community Land Model development, *J. Geophys. Res.*, *113*, G01025, doi:10.1029/2007JG000562.

1. Introduction

[2] The land surface provides a lower boundary to the atmosphere for exchanges of radiation, heat, water, momentum and chemical species such as CO_2. The importance of these exchanges for the climate system is increasingly being recognized [*Betts et al.*, 2000; *Cox et al.*, 2000; *Pielke*, 2001; *Friedlingstein et al.*, 2003; *Seneviratne et al.*, 2006; *Betts et al.*, 2007]. Storage of heat and water on land constitutes a significant memory component within the climate system. For instance, soil moisture has strong controls on ecosystem function and boundary layer processes in regions where evapotranspiration as a biophysical process is limited by soil moisture availability [*Seneviratne and Stöckli*, 2007]. Furthermore the global carbon cycle interacts with soil and vegetation biophysics since carbon assimilation and ecosystem respiration are regulated by the land surface radiation, water and heat balances.

[3] Land surface models for use in global climate models have been developed over the last three decades. They range from simple energy balance parameterizations to complex schemes including the full terrestrial biogeochemical cycle [*Sellers et al.*, 1997; *Friedlingstein et al.*, 2006] and are based on knowledge gained from field and laboratory research in plant physiology, soil science and micrometeorology. However, many model components resulted from relatively few observations and from idealized laboratory experiments. This leads to significant uncertainty in the parameterization of processes which are now employed on a global scale for studying land-climate interaction at seasonal to decadal timescales.

[4] These model uncertainties have been documented in model inter-comparison studies (e.g., PILPS [*Henderson-Sellers et al.*, 1996; *Pitman et al.*, 1999; *Nijssen et al.*, 2003]). Large differences still exist in the simulation of

[1]Department of Atmospheric Science, Colorado State University, Fort Collins, Colorado, USA.
[2]Climate Services, Federal Office of Meteorology and Climatology MeteoSwiss, Zürich, Switzerland.
[3]NASA Earth Observatory, Goddard Space Flight Center, Greenbelt, Maryland, USA.
[4]Terrestrial Sciences Section, National Center for Atmospheric Research, Boulder, Colorado, USA.
[5]Department of Geological Sciences, University of Texas at Austin, Austin, Texas, USA.
[6]Numerical Terradynamics Simulation Group, University of Montana, Missoula, Montana, USA.

0148-0227/08/2007JG000562$09.00

seasonal and annual evapotranspiration and runoff dynamics [*Gedney et al.*, 2000]. It is not clear how much present climate model predictions are affected by these limitations. For instance, coupling strength between the land surface and the atmosphere varies not only by region but also by the used parameterization [*Koster et al.*, 2004]. A realistic representation of land surface responses to climatic variability as part of global climate simulations is important for future climate impact studies. It is also mandatory in the prediction of the global carbon balance, with regional sinks and sources, which will be part of the next generation earth system models.

[5] The Community Land Model version 3 (CLM3.0) is a community-developed land surface model maintained at NCAR (National Center for Atmospheric Research) and includes a comprehensive set of mechanistic descriptions of soil physical and vegetation biophysical processes [*Oleson et al.*, 2004]. The model can be extended to a full biogeochemical description of the terrestrial carbon-nitrogen interactions [*Thornton et al.*, 2007] based on the BIOME-BGC model and vegetation biogeography with disturbance dynamics [*Levis et al.*, 2004] based on the LPJ model.

[6] Despite being an advanced process-based land surface model, CLM3.0 has known deficiencies in simulating the long term terrestrial hydrological cycle in climate simulations. They can influence the surface climate and vegetation biogeography through plant-soil carbon and water dynamics [*Dickinson et al.*, 2006]. In coupled simulations with many feedback processes, these shortcomings can further amplify errors from the atmospheric model, with unhealthy consequences for the simulated climate system and land-atmosphere interactions [*Bonan and Levis*, 2006; *Hack et al.*, 2006; *Lawrence et al.*, 2007]. The CLM model development community has proposed a number of improved soil hydrological and plant physiological formulations that represent previously missing processes that appear to be responsible for a damped soil water storage cycle in the tropics and the generally dominating fraction of bare soil evaporation to plant transpiration [see, e.g., *Lawrence et al.*, 2007]. For details about the full set of proposed changes to CLM, see *Oleson et al.* [2007]. Here, we both evaluate how these changes have improved the model and also elucidate how the use of FLUXNET data has contributed to the identification of deficiencies in the model including the aforementioned missing processes. The subset of changes to the model evaluated in detail here include: (1) a Topmodel-based runoff, infiltration and aquifer model, (2) a bare soil evaporation resistance and, (3) an empirical function for nitrogen control of the photosynthesis-conductance formulation. The aim of this study is to individually implement and evaluate the proposed algorithms and to quantify their impact on the simulated terrestrial carbon and water cycle on hourly to seasonal timescales.

[7] Such a study is difficult for a global land surface model due to a lack of suitable global observations [*Henderson-Sellers et al.*, 2003]. However, long-term ground-based ecosystem observations such as FLUXNET [*Baldocchi et al.*, 2001], the global network of research sites where the eddy covariance technique is used to monitor surface-atmosphere exchanges of carbon, water, and energy, are a unique data source for process-based land surface model development [*Running et al.*, 1999; *Canadell et al.*, 2000; *Reichstein et al.*, 2002; *Turner et al.*, 2004; *Stöckli and Vidale*, 2005; *Bogena et al.*, 2006; *Friend et al.*, 2007] although it is important to remember that these observations are of local scale and can be subject to potentially large random and systematic errors [*Wilson et al.*, 2002; *Foken*, 2008]. FLUXNET is probably the most comprehensive terrestrial ecosystem data set today, and uncertainties in radiation, heat, water and carbon flux measurements can be accurately quantified [*Falge et al.*, 2001; *Schmid*, 2002; *Hollinger and Richardson*, 2005; *Richardson et al.*, 2006]. Flux tower observations per se only have limited spatial scalability and do not provide a gridded global coverage. They do, however, span a global range of ecosystems where we can exercise land surface models like CLM3.0. The importance of individual processes regulating the heat, water and carbon exchanges varies by climate. Certain processes may only play a role at one end of the multidimensional spectrum of climatic environments.

[8] In this study we use 15 FLUXNET tower sites from the temperate, mediterranean, tropical, north boreal and subalpine climate zones to interactively assess the realism of proposed CLM3.0 enhancements during model development. Gap-filled yearly meteorological forcing data sets at the tower sites are used to conduct off-line single-point simulations. In the results section quality-screened heat, water and carbon fluxes as well as soil moisture and soil temperature measurements are compared to simulated equivalents. Several model hydrological deficiencies controlling turbulent surface fluxes, are successively identified and corrected with this study. It is therefore demonstrated how FLUXNET helps to reduce model biases in the simulation of land surface processes and how it can be used as an efficient tool for the reevaluation of land surface models like CLM3.0 during their development stage.

2. Methods

2.1. Model

[9] CLM3.0 (Community Land Model Version 3 [*Oleson et al.*, 2004]) is the land model component of CCSM3 (Community Climate System Model Version 3 [*Collins et al.*, 2006]). It includes mechanistic formulations of physical, biophysical and biogeochemical processes that simulate the terrestrial radiation, heat, water and carbon fluxes in response to climatic forcings. CLM3.0 provides an integrated coupling of photosynthesis, stomatal conductance, and transpiration. Therefore vegetation biophysical processes strongly interact with soil hydrological processes. The CLM3.0 community has proposed a number of model changes as a response to the above discussed deficiencies of the CLM3.0 code. Three of them, in particular, are directly related to simulations of the global hydrological cycle and are summarized here (full documentation in *Oleson et al.* [2007]):

[10] 1. Infiltration, runoff and groundwater: A Topmodel-based infiltration, saturation and runoff scheme [*Beven and Kirkby*, 1979; *Niu et al.*, 2005] introduces catchment-scale soil water dynamics from classical hydrological modeling to a land surface model for global applications. Additionally, a prognostic aquifer scheme [*Niu et al.*, 2007] allows for seasonal to inter-annual soil water storage fluctuations which involve soil depths beyond the 3.43 m deep soil of

Table 1. Flux Towers Used in This Study[a]

Number	Site	Lon [°E]	Lat [°N]	Alt (Hgt) [m]	Biome Type	Soil Type	Years	Climate Zone
			CarboEurope					
1	Vielsalm [*Aubinet et al.*, 2001]	6.00	50.30	450 (40)	MF	loam	1997–2005	Temperate
2	Tharandt [*Grunwald and Bernhofer*, 2007]	13.57	50.96	380 (42)	ENF	loam	1998–2003	Temperate
3	Castel Porziano [*Valentini*, 2003]	12.38	41.71	68 (25)	EBF	loamy sand	2000–2005	Mediterranean
4	Collelongo [*Valentini*, 2003]	13.59	41.85	1550 (32)	DBF	silt loam	1999–2003	Mediterranean
5	Kaamanen [*Laurila et al.*, 2001]	27.30	69.14	155 (5)	TUN	loam	2000–2005	North boreal
6	Hyytiälä [*Suni et al.*, 2003]	24.29	61.85	181 (23)	ENF	loamy sand	1997–2005	Boreal
7	El Saler [*Ciais et al.*, 2005]	−0.32	39.35	10 (15)	ENF	loamy sand	1999–2005	Mediterranean
			LBA					
8	Santarem KM83 [*Goulden et al.*, 2004]	−54.97	−3.02	130 (64)	EBF	sandy clay	2001–2003	Tropical
9	Tapajos KM67 [*Hutyra et al.*, 2007]	−54.96	−2.86	130 (63)	EBF	clay	2002–2005	Tropical
			AmeriFlux					
10	Morgan Monroe [*Schmid et al.*, 2000]	−86.41	39.32	275 (46)	DBF	clay loam	1999–2005	Temperate
11	Boreas OBS [*Dunn et al.*, 2007]	−98.48	55.88	259 (30)	ENF	clay loam	1994–2005	Boreal
12	Lethbridge [*Flanagan et al.*, 2002]	−112.94	49.71	960 (4)	GRA	silt loam	1998–2004	Boreal
13	Fort Peck [*Gilmanov et al.*, 2005]	−105.10	48.31	634 (4)	GRA	sandy loam	2000–2005	Temperate
14	Harvard Forest [*Urbanski et al.*, 2007]	−72.17	42.54	303 (30)	DBF	sandy loam	1994–2003	Temperate
15	Niwot Ridge [*Monson et al.*, 2002]	−105.55	40.03	3050 (26)	ENF	clay	1999–2004	Subalpine

[a]Biome types: mixed forest (MF), evergreen needleleaf forest (ENF), deciduous broadleaf forest (DBF), tundra (TUN), evergreen broadleaf forest (EBF), grasslands (GRA). Alt is the elevation of the tower above the sea level, and Hgt is the approximate height of the wind/temperature and flux measurements above the surface.

CLM3.0. The depth of the water table is highly related to subsurface runoff magnitude [*Sivapalan et al.*, 1987; *Chen and Kumar*, 2001]. During dry periods the aquifer contributes to base-flow and provides a long-term storage for soil water. It is hydraulically connected to the root zone and therefore interacts with vegetation biophysical state and function. During rainfall events or in moist climates the water table can rise into the model soil column, which increases root zone soil moisture and subsurface runoff. It also increases infiltration since soil hydraulic conductivity shows a highly nonlinear dependence on soil water content. In the original CLM3.0 the magnitude of soil water dynamics is constrained to total soil depth, while here the aquifer acts as a buffer with a storage capacity varying by climate, soil, vegetation and topography.

[11] 2. Soil evaporation: In the original CLM3.0 an unreasonably high fraction of evapotranspiration comes from bare soil evaporation [*Lawrence et al.*, 2007]. In addition to the already simulated top soil humidity [*Oleson et al.*, 2007, equations (F1)–(F4)] a new resistance function was implemented, based on work by *Sellers et al.* [1992]. Equation (F5) in *Oleson et al.* [2007] is an empirical parameterization of the bare soil evaporation resistance, which was developed on a limited number of FIFE 87 measurements. It had previously been successfully used in SiB 2 and 2.5 (Simple Biosphere Model Versions 2 and 2.5 [*Sellers et al.*, 1996; *Vidale and Stöckli*, 2005]).

[12] 3. Nitrogen limitation: Initial simulations including the above soil hydrological processes revealed an exaggerated light response of photosynthesis, resulting in too much primary production and slightly overestimated latent heat flux. Apart from soil water, temperature, humidity and radiation, leaf nitrogen content can define the maximum rate of carboxylation in the photosynthesis formulation and therefore stomatal opening. While prognostic nitrogen is part of the separately developed biogeochemistry scheme CLM-CN [*Thornton et al.*, 2007], many applications require the standard CLM. In order to simulate nitrogen control on photosynthesis and therefore stomatal conductance, PFT-dependent factors $f(N)$ were diagnosed from a simulation employing CLM-CN from a fully spun-up preindustrial state of terrestrial biogeochemistry. $f(N)$ represents the proportion of potential photosynthesis that is realized in the face of nitrogen limitation, as predicted by CLM-CN. For our simulations $f(N)$ is imposed on the maximum rate of carboxylation V_{max} in a similar manner to, e.g., plant water stress, as described in *Oleson et al.* [2007, Appendix G]. V_{max} then modulates canopy photosynthesis and therefore carbon uptake as well as canopy conductance and therefore transpiration in the model.

2.2. Data

[13] FLUXNET is a global network of currently more than 400 flux towers which operate independently or as part of regional networks (CarboEurope, AmeriFlux, LBA, etc.). The off-line single point simulations with CLM3.0 were carried out at 15 FLUXNET sites covering a range of climatic environments listed in Table 1: temperate (5), mediterranean (3), boreal (3), tropical (2), north boreal (1) and subalpine (1). Only towers providing three or more years of continuous driver and validation data as part of the publicly accessible AmeriFlux or CarboEurope standardized Level 2 database have been selected. In order to obtain a balanced set of flux towers, only a few temperate sites could be used. On the other hand arctic and especially more arid sites with multiyear continuous coverage were difficult to find.

2.2.1. Forcing Data

[14] Yearly gap-filled meteorological driver data were created from level 2 flux tower data sets at 30 or 60 min time steps. For off-line simulations the model requires RG_d (downwelling short-wave radiation; W m^{-2}), LW_d (downwelling long-wave radiation; W m^{-2}), T_a (air temperature; K), RH_a (relative humidity; %), u (wind speed; m s^{-1}), P_s (surface pressure; Pa), P (rainfall rate; mm s^{-1}). Measurements of these quantities at the tower reference height

(Table 1) were used. Outliers which deviated $n\sigma$ times from the median-filtered time series were removed (σ is the standard deviation of the original time series and n = 4, except for RH_a where n = 8; for u where n = 20 and for LW_d where n = 16). Up to two month long successive gaps were filled by applying a 30 day running mean diurnal cycle forwards and backwards through the yearly time series. Years with more than 2 month of consecutive missing data were not used.

[15] The following exceptions were applied to the above procedure:

[16] 1. RG_d was not median-filtered since most of its variability occurs on diurnal timescale. Instead the potential solar radiation as a function of latitude and local solar time, scaled with the annual maximum observed RG_d, provided an upper bound for RG_d.

[17] 2. P was neither median-filtered nor gap-filled. Where provided by tower sites, daily precipitation totals from nearby stations were used to replace missing 30 or 60 min tower data. Daily precipitation totals were evenly distributed at night between 00:00–04:00 during days when no daily 30 or 60 min were available; and they were used to augment valid 30 and 60 min data during days with partial missing data periods.

[18] 3. For sites with no P_s, it was estimated by

$$P_s = P_{s_0} e^{-\frac{Mgz}{RT_a}}, \tag{1}$$

where P_{s_0} is the mean sea level pressure (101300 Pa), M is the molecular weight of air (0.029 kg mol^{-1}), g is the gravitational acceleration (9.81 m s^{-2}), z is the tower height above sea level (m) and R is the universal gas constant (8.314 J K^{-1} mol^{-1}).

[19] 4. For sites with no LW_d (most sites), it was estimated from the surface radiation balance:

$$LW_d = R_n - RG_d + RG_u + \sigma\left(\frac{T_a + T_r}{2}\right)^4, \tag{2}$$

where R_n and RG_u are non-gap-filled net radiation (Wm^{-2}) and upwelling solar radiation (Wm^{-2}), σ is the Stefan-Bolzmann constant ($5.67 \cdot 10^{-8}$ Wm^{-2}K^{-4}) and T_r is either the canopy temperature or soil surface temperature (K), depending on data availability. As a backup algorithm (any of the right hand side variables in equation (2) missing, most sites, again) downwelling long-wave radiation was estimated by using the clear-sky LW_d parameterization by *Idso* [1981], modified by an emissivity correction factor as proposed by *Gabathuler et al.* [2001]:

$$LW_d = \epsilon_c \epsilon_0 \sigma T_a^4, \tag{3}$$

where:

$$\epsilon_c = 1 + 0.3(1 - K_0)^2 \quad \text{and} \tag{4}$$

$$\epsilon_0 = 0.7 + e_a \cdot 5.95 \cdot 10^{-5} e^{\frac{1500}{T_a}}, \tag{5}$$

where ϵ_0 is the clear sky atmospheric emissivity as a function of T_a and atmospheric vapor pressure e_a (mb). ϵ_c adjusts ϵ_0 for cloud cover. It depends on the clearness index K_0, which ranges from 0 to 1 (full cloud cover to clear sky). K_0 can be approximated by dividing measured by potential downwelling solar radiation, but only during daytime. We replaced all nocturnal K_0 values where RG_d was below 50 W m^{-2} with linearly interpolated values. While clear sky LW_d can be reasonably estimated the above formulation for all-sky LW_d is a rough fix in need of some data. Since cloud emissivity depends on, e.g., cloud type, water content and cloud vertical extent an uncertainty of roughly 5–20 W m^{-2} is introduced to the driver data set [*Gabathuler et al.*, 2001] by using this algorithm.

[20] The consistently gap-filled meteorological forcing data from the above 15 sites (and from around 50 additional sites) are available from the authors (upon request also as ALMA-compliant NetCDF files).

2.2.2. Validation Data

[21] Turbulent surface fluxes and soil physical state variables from the Level 2 flux tower data sets were used to validate the model during the implementation stage of above-described modifications. None of the validation data were gap-filled since our intention was to look at timing and phase of the seasonal fluxes in response to climatic forcings rather than to match the local-scale heat, water and carbon balance at the end of the year. LE (latent heat flux; W m^{-2}), H (sensible heat flux; W m^{-2}), and NEE (net ecosystem exchange; μmol m^{-2} s^{-1}) were u* filtered in order to account for the well documented biases in eddy covariance measurements during periods of low turbulence [*Schmid et al.*, 2003]: comparisons to modeled fluxes were only performed for times when the u* value was above 0.2 m s^{-1} (in the mean 67.4% of the data). Ideally, the u* threshold should be site-dependent and would only need to be applied to nocturnal data. Random uncertainties in turbulent surface fluxes [*Hollinger and Richardson*, 2005] were estimated based on empirical findings by *Richardson et al.* [2006]. Systematic errors in measured surface fluxes due to failure in energy balance closure were accounted for by multiplying u*-screened surface fluxes with the residual of the energy balance closure (as % of R_n) for each site, which was calculated from the regression of hourly observed R_n versus LE and H fluxes [*Wilson et al.*, 2002; *Grunwald and Bernhofer*, 2007]. In all LE and H plots, the total errors were calculated as the square root of the sum of the squares of random and systematic errors for each analysis time step (e.g., hourly or monthly). Table 2 presents a summary of these uncertainty estimates for each site.

[22] The model in its standard configuration simulates GPP (gross primary productivity; μmol m^{-2} s^{-1}) but not R_e (ecosystem respiration; μmol m^{-2} s^{-1}). In order to calculate NEE (net ecosystem exchange; μmol m^{-2} s^{-1}), which is the difference between two large terms GPP and R_e, both terms would need to be accurately prognosed. This requires a mechanistic formulation involving prognostic carbon and nitrogen fluxes and pools as for instance presented by *Thornton et al.* [2007]. In order to compare modeled carbon uptake to observations, observed estimates of GPP were empirically derived from observed NEE, PAR (photosynthetically active radiation; μmol m^{-2} s^{-1}), and T_s (5 cm soil

Table 2. Uncertainty of Observations: % of u* Filtered Data (u*), % of Energy Balance Closure (ebc), Mean Error in LE Due to Failure of Energy Balance Closure (ebc LE), Mean Random Error in LE (ran LE), Mean Error in H Due to Failure of Energy Balance Closure (ebc H), and Mean Random Error in H (ran H)

Number	Site	u* %	ebc %	ebc LE W m^{-2}	ran LE W m^{-2}	ebc H W m^{-2}	ran H W m^{-2}
1	Vielsalm	21	73	7.0	20.2	7.5	29.7
2	Tharandt	44	78	8.4	24.5	7.7	29.8
3	Castel Porziano	34	83	8.6	25.7	13.9	36.6
4	Collelongo	41	81	8.8	28.1	12.3	37.1
5	Kaamanen	56	72	10.4	23.9	3.4	22.9
6	Hyytiälä	47	72	8.3	21.5	6.2	26.1
7	El Saler	24	83	7.8	25.6	12.3	39.1
8	Santarem KM83	47	81	32.7	59.2	8.6	27.7
9	Tapajos KM67	36	81	24.9	44.9	6.5	26.3
10	Morgan Monroe	22	65	18.8	28.2	11.0	29.5
11	Boreas OBS	25	80	5.8	20.7	10.4	31.1
12	Lethbridge	42	77	7.3	21.8	8.8	34.3
13	Fort Peck	42	68	13.6	24.6	13.2	30.3
14	Harvard Forest	17	84	6.9	24.9	6.4	31.1
15	Niwot Ridge	17	76	12.7	27.6	12.3	40.7

temperature; K) using the algorithms by *Desai et al.* [2005]. Measured volumetric soil moisture was converted to percent saturation by assuming a porosity of 0.48 and by using the model soil layer which was closest to observation depth.

2.3. Experiment

[23] Single point model simulations were performed for each of the 15 flux tower sites. The original model (CLM3.0) was successively modified with the proposed changes:

[24] 1. CLM3.0: the original and publicly available release code of CLM3.0.

[25] 2. CLMgw: addition of a Topmodel-based infiltration, runoff and aquifer storage formulation to CLM3.0. CLMgw (gw stands for groundwater) further includes all other major updates in the model (e.g., a new canopy integration scheme, canopy interception changes, new frozen soil and plant soil water availability parameterizations) as described in *Oleson et al.* [2007] which were not part of the original CLM3.0.

[26] 3. CLMgw_rsoil: addition of the bare soil evaporation resistance formulation to CLMgw (rsoil stands for soil resistance).

[27] 4. CLM3.5: addition of a PFT-dependent nitrogen limitation factor to CLMgw_rsoil. This simulation is equivalent to the public release code of CLM3.5.

2.3.1. Boundary Conditions

[28] Vegetation and soil parameters for each site were derived from the standard CLM3.0 PFT-dependent look-up tables based on vegetation type and soil type (constant vertical profiles of sand/clay fractions for each site) from Table 1. A single PFT was used for each site. Visible and

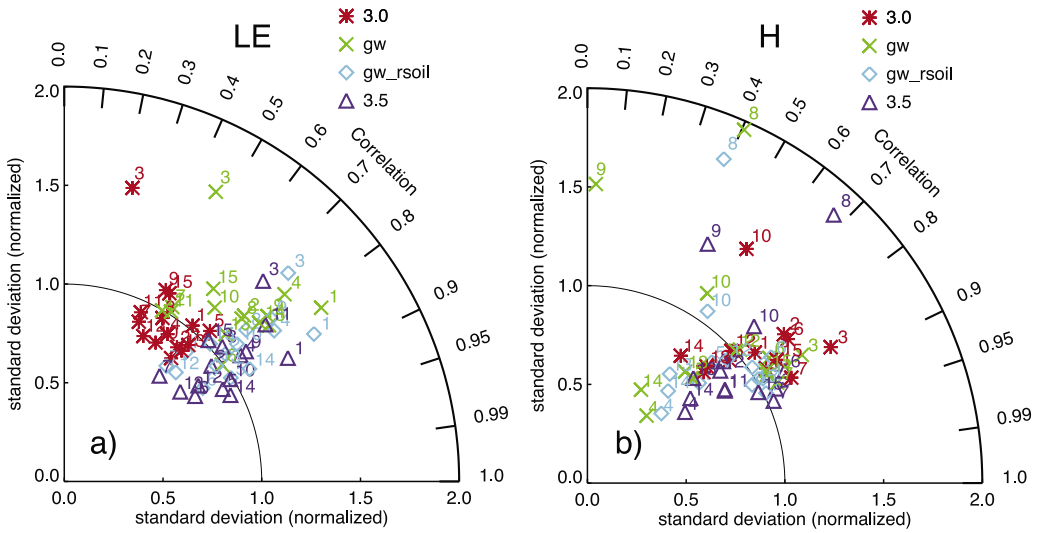

Figure 1. Performance of four model versions at 15 FLUXNET towers (numbers 1–15). Statistics in the Taylor diagram are derived from hourly simulated and observed LE and H fluxes. Legend: CLM3.0: red asterisks; CLMgw: green crosses; CLMgw_rsoil: cyan diamonds; CLM3.5: violet triangles. In CLM3.0 H is off-scale for the two tropical sites 8 and 9 (and therefore not shown).

Table 3. Performance of Simulated LE and H Fluxes in Four CLM Versions (3.0, gw, gw_rsoil, 3.5): R and RMSE (W m^{-2}, in Brackets) are Diagnosed on Hourly and Monthly Timescales[a]

		LE				H			
Number	Site	3.0	gw	gw_rsoil	3.5	3.0	gw	gw_rsoil	3.5
				Hourly					
1	Vielsalm	0.68 (43.0)	0.84 (57.1)	0.88 (46.1)	**0.90 (35.9)**	0.79 (67.0)	0.71 (67.1)	0.74 (63.9)	**0.83 (54.2)**
2	Tharandt	0.65 (44.3)	0.74 (51.4)	**0.79** (37.2)	**0.79 (35.2)**	0.80 (75.3)	0.75 (75.3)	0.82 (60.8)	**0.86 (55.4)**
3	Castel Porziano	0.23 (89.7)	0.46 (86.8)	**0.73** (66.5)	0.70 (**61.6**)	0.87 (102.1)	0.86 (93.3)	0.86 (78.4)	**0.89 (68.8)**
4	Collelongo	0.57 (70.7)	0.76 (87.2)	**0.81** (67.7)	**0.81 (55.3)**	0.72 (91.2)	0.66 (109.0)	0.73 (97.7)	**0.81 (83.0)**
5	Kaamanen	0.71 (40.6)	0.81 (40.2)	0.86 (27.2)	**0.88 (25.2)**	**0.76 (37.9)**	0.70 (39.0)	0.72 (40.2)	0.74 (39.3)
6	Hyytiälä	0.65 (39.6)	0.80 (32.5)	0.83 (28.7)	**0.84 (28.3)**	0.81 (59.1)	0.82 (50.9)	0.82 (52.5)	**0.87 (47.6)**
7	El Saler	0.42 (68.4)	0.53 (65.4)	0.66 (50.2)	**0.67 (49.5)**	0.89 (95.7)	0.88 (87.7)	0.89 (81.1)	**0.91 (75.4)**
8	Santarem KM83	0.52 (157.8)	0.74 (135.2)	**0.77** (127.1)	0.76 (**111.9**)	0.59 (166.1)	0.41 (125.1)	0.39 (118.0)	**0.68 (92.0)**
9	Tapajos KM67	0.47 (147.2)	0.78 (132.6)	0.78 (131.0)	**0.81 (100.2)**	**0.45** (146.7)	0.03 (120.7)	−0.02 (120.5)	**0.45 (83.1)**
10	Morgan Monroe	0.55 (89.8)	0.66 (102.5)	0.78 (76.5)	**0.85 (58.5)**	0.56 (111.7)	0.53 (98.7)	0.57 (88.7)	**0.73 (75.1)**
11	Boreas OBS	0.41 (49.6)	0.53 (45.7)	0.69 (**35.6**)	**0.79** (41.2)	0.84 (68.4)	**0.86** (65.1)	0.85 (**63.7**)	0.83 (70.8)
12	Lethbridge	0.48 (53.7)	0.50 (56.4)	0.72 (40.1)	**0.81 (32.5)**	0.74 (82.1)	0.75 (81.5)	0.75 (78.7)	**0.76 (74.3)**
13	Fort Peck	0.67 (60.6)	0.74 (58.9)	**0.80** (48.0)	0.79 (**47.5**)	**0.71** (63.3)	0.66 (69.1)	0.60 (72.9)	**0.71 (63.2)**
14	Harvard Forest	0.67 (62.8)	0.78 (68.8)	0.86 (46.6)	**0.89 (37.5)**	0.59 (96.7)	0.51 (104.5)	0.67 (88.0)	**0.79 (73.8)**
15	Niwot Ridge	0.49 (66.1)	0.61 (63.0)	**0.73 (46.4)**	0.71 (47.6)	0.84 (96.7)	0.85 (85.9)	0.86 (78.9)	**0.88 (72.5)**
				Monthly					
1	Vielsalm	0.73 (**22.0**)	0.91 (36.9)	**0.96** (29.0)	**0.96** (23.1)	0.85 (30.3)	0.81 (22.0)	0.85 (20.0)	**0.88 (19.6)**
2	Tharandt	0.83 (15.9)	0.88 (25.6)	**0.93** (13.6)	**0.93** (**11.2**)	0.88 (35.0)	0.84 (33.4)	**0.89 (20.2)**	0.88 (21.9)
3	Castel Porziano	−0.21 (44.2)	0.05 (51.3)	0.79 (37.3)	**0.81** (**31.3**)	**0.97** (41.3)	0.96 (44.5)	0.96 (34.4)	**0.97 (28.6)**
4	Collelongo	0.61 (37.1)	0.88 (47.1)	**0.92** (33.8)	**0.92** (**26.9**)	0.76 (73.4)	0.71 (47.0)	0.73 (37.1)	**0.79 (29.2)**
5	Kaamanen	0.88 (16.2)	0.91 (18.6)	0.95 (11.4)	**0.96** (**10.4**)	**0.92** (14.4)	0.89 (**13.2**)	0.90 (17.0)	0.90 (17.9)
6	Hyytiälä	0.89 (14.2)	0.94 (11.1)	**0.97 (7.4)**	**0.97** (8.6)	0.88 (28.7)	**0.92** (**21.0**)	**0.92** (23.4)	0.91 (24.9)
7	El Saler	0.31 (29.3)	0.54 (22.4)	0.71 (**18.3**)	**0.72** (18.4)	0.95 (47.1)	0.95 (36.6)	0.95 (**34.5**)	0.95 (36.1)
8	Santarem KM83	0.33 (85.5)	0.65 (65.0)	**0.69** (57.9)	0.66 (**55.1**)	**0.43** (72.9)	0.03 (71.7)	0.04 (71.7)	0.18 (**44.1**)
9	Tapajos KM67	0.03 (65.5)	0.65 (76.8)	**0.69** (74.2)	0.68 (**55.5**)	**0.36** (61.4)	−0.23 (60.2)	−0.29 (58.1)	−0.22 (**40.8**)
10	Morgan Monroe	0.74 (41.7)	0.85 (53.4)	**0.95** (33.1)	**0.95** (**27.8**)	0.26 (48.6)	0.41 (37.7)	0.41 (37.7)	**0.43 (25.2)**
11	Boreas OBS	0.75 (18.0)	0.76 (17.1)	0.89 (**12.0**)	**0.96** (20.8)	0.93 (18.5)	**0.95** (18.7)	**0.95 (16.7)**	0.92 (33.9)
12	Lethbridge	0.77 (22.0)	0.71 (23.8)	0.83 (19.5)	**0.92** (**12.4**)	0.90 (26.5)	0.91 (26.7)	0.91 (24.8)	**0.92 (21.2)**
13	Fort Peck	0.79 (32.4)	0.81 (29.4)	**0.84** (**27.1**)	0.83 (28.5)	**0.84** (**22.5**)	0.74 (31.5)	0.59 (35.7)	0.79 (27.0)
14	Harvard Forest	0.70 (28.1)	0.86 (23.7)	**0.96** (**11.5**)	0.95 (14.5)	0.30 (39.8)	0.23 (46.3)	0.55 (33.9)	**0.49 (32.4)**
15	Niwot Ridge	0.50 (26.3)	0.72 (21.2)	**0.90** (**13.5**)	0.88 (14.4)	0.72 (41.4)	0.80 (30.0)	**0.84** (**22.8**)	0.82 (23.9)

[a]Bold numbers show the best of the four model versions for each diagnostic and site.

near-infrared soil albedos were set to arbitrary values of 0.18/0.36 for a dry top soil and 0.09/0.18 for a saturated top soil due to a lack of in-situ information at most sites. Stem Area Index was set to 0.08. Vegetation top/bottom heights were 35 m/1 m for tropical forests, 20m/10m for other forests, and 1 m/0.1 m for short vegetation. A climatological monthly Leaf Area Index for each site came from the 1982–2001 EFAI-NDVI data set [*Stöckli and Vidale*, 2004]. Since our intent was to perform a process-based analysis of a global model, PFT-dependent model parameters were not tuned to site-specific and species-specific conditions.

2.3.2. Initial Conditions and Spin-Up

[29] The model was initialized from its standard arbitrary initial conditions of 283 K vegetation, ground and soil temperatures, 30% (CLM3.0) 40% (CLMgw, CLMgw_rsoil, CLM3.5) volumetric soil water content and with empty ground snow and canopy interception water stores. Spin-up was achieved by repeating the full range of available years five times for each site (five spin-up cycles). Mean yearly latent and sensible heat fluxes were within 0.1 W m^{-2} of those from the previous spin-up cycle after a single spin-up cycle (similar to PILPS 2a spin-up criteria [*Chen et al.*, 1997]). More arid climates would need longer spin-up times since the water table there takes longer to adjust (see, e.g., the global simulations by *Oleson et al.* [2008]). Nevertheless, surface fluxes are not affected by variations of a very deep water table in such areas.

2.3.3. Analysis

[30] Hourly model output from the last spin-up cycle was used for the analysis. At sites where 30 min measurements were available they were averaged to 60 min values.

3. Results

[31] Comparisons between modeled and observed LE and H in Figure 1 (Taylor Diagram) and Table 3 (R and RMSE) provide a quick overview of performance changes across model versions: the original CLM3.0; modifications using a groundwater scheme (CLMgw), addition of a bare soil evaporation resistance (CLMgw_rsoil) and further addition of PFT-dependent nitrogen limitation factor in the final model version (CLM3.5). (In the Taylor diagram [*Taylor*, 2001], four statistical quantities are geometrically connected: the correlation coefficient R, standard deviation of observations σ_o, standard deviation of the model σ_m, and the centered pattern root-mean-square error E'. The polar axis displays R and the radial axes display the standard deviation of the modeled variable divided by the standard deviation of the observed variable σ_m/σ_o. The geometric relationship of this diagram is such that the distance between the 1.0 value of the X-axis and the plotted value show E' and thus is a measure for the absolute model error. Root-mean-square error E is given by: $E = \overline{E} + E'$, where $\overline{E}$ is the mean bias. The four statistical moments are connected

by: $E'^2 = \sigma_m^2 + \sigma_o^2 - 2\sigma_m\sigma_o R$.) General changes in LE and H on the hourly and monthly timescale covering all sites are discussed first, followed by a close inspection of results at individual sites encompassing temperate, north boreal, mediterranean and the tropical ecosystems.

3.1. Latent Heat Flux

[32] The R of LE shown in Figure 1a increases with the new groundwater scheme (CLMgw, green crosses) compared to the original CLM3.0 (red asterisks). However, the variability of LE is now exaggerated compared to observations. The inclusion of the bare soil evaporation resistance (CLMgw_rsoil, cyan diamonds) generates more realistic LE variability, resulting in a higher R than with the groundwater formulation alone. A further improvement in both correlation and variability is achieved with the nitrogen limitation (CLM3.5, violet triangles). R for hourly LE at most sites increases from around 0.4–0.7 (CLM3.0) and 0.5–0.8 (CLMgw) to 0.7–0.9 (CLMgw_rsoil and CLM3.5). For all 15 sites hourly and monthly LE has a higher R and a lower RMSE for CLM3.5 compared to CLM3.0. Some sites display substantial improvements: e.g., the mediterranean site Castelporziano (R increases from 0.23 to 0.70 for hourly LE and from −0.21 to 0.81 for monthly LE) and the tropical site KM67 (R for hourly LE increases from 0.47 to 0.81; and for monthly LE from 0.03 to 0.68). Similarly, temperate ecosystems show a steady improvement (e.g., Vielsalm or Morgan Monroe). High latitude ecosystems (e.g., Kaamanen and Hyytiälä) are already well simulated by CLM3.0, but they also slightly improve. RMSE decreases at all sites (except for Vielsalm at the monthly timescale) from CLM3.0 to CLM3.5 on both hourly and monthly timescale. The grassland sites Lethbridge and Fort Peck improve on both hourly and monthly timescale, but to a lesser extent than forest sites.

3.2. Sensible Heat Flux

[33] The changes in H, shown in Figure 1b, are not as easily generalized as LE, although the model changes appear to result in an overall improvement. Even though changes in LE are almost fully compensated by opposite changes in H, the new hydrology formulations do not affect R of H as much. This is due to a number of factors. First of all, H is smaller than LE for most sites. Secondly, while LE can completely be shut down by soil moisture, H is strongly coupled to net shortwave radiation through skin temperature, largely independent of the state of subsurface hydrology [*Betts*, 2004]. R is a good indicator for phase but not for magnitude in this case. For sites like Castelporziano, where the R of LE increased substantially, R of H remains constant (R increases from 0.87 to 0.89; hourly timescale). But RMSE of H decreases from 102.1 W m^{-2} to 68.8 W m^{-2}. Remaining high RMSE values should also be viewed with respect to uncertainties in observed fluxes (Table 2). This result suggests that the mean error and variability of H was improved with the new hydrology, and not the timing and phase of H. Indeed, in Figure 1b R values remain roughly the same for all four model versions. But the spread in the radial direction decreases and successively moves symbols closer towards observed variability at the 1.0 arc by use of the new formulations. Several sites actually show a slightly worse R with the new hydrology, but they still have a decreased RMSE compared to CLM3.0. For the two tropical sites hourly R for H becomes worse in CLMgw and CLMgw_rsoil and increases again with CLM3.5. Hourly and monthly RMSE for those sites significantly decreases by around 35–45%. Only small changes in R and RMSE on both hourly and monthly timescale can be seen for the two grasslands Fort Peck and Lethbridge. They cannot make use of the groundwater if the water table falls below their shallow rooting depth, which is most likely the case at those two sites.

3.3. Temperate

[34] Morgan Monroe State Forest is a deciduous temperate broadleaf forest in Indiana (USA). Monthly mean measured LE (Figure 2c; black) displays a clear seasonal cycle with a growing season between May and October. H (Figure 2d; black) peaks before leaf emergence in March and April [*Schmid et al.*, 2003].

[35] CLM3.0 shows excess LE in winter and too low LE in summer. This results in a too low modeled variability of hourly LE and exaggerated variability of hourly H (Figure 2b; red). The modeled root zone soil moisture is low throughout the year compared to observed soil moisture (Figure 2a; black and red). The simulated soil moisture profile (Figure 3a; CLM3.0) provides insight into the processes responsible for these results: an impermeable and dry soil layer is formed after a few years of spin-up and inhibits further infiltration and water storage at deeper soil moisture levels. The main reason for this effect is found in the delicate interplay between soil physics and the numerical solution of the vertical soil water transfer. As discussed in *Stöckli et al.* [2007], the exponential relationship between soil hydraulic conductivity and soil water content in a finite difference numerical solution of Darcy's equation can create a feedback below certain soil water levels which successively decouples upper from lower soil layers through further inhibition of infiltration. We can see in Figure 3a that this "vicious loop" cannot be broken even by long precipitation events during spring.

[36] It was chosen to improve the physical and biophysical processes in order to support a stable numerical solution of soil water dynamics as documented in *Oleson et al.* [2007]: a Topmodel-based surface and subsurface runoff scheme [*Niu et al.*, 2005] coupled to a prognostic groundwater scheme [*Niu et al.*, 2007] are mechanistic formulations of soil water dynamics which were not in the original CLM3.0. The new groundwater scheme (Figure 3b; CLMgw) increases soil moisture to a range where the numerical solution provides a more stable interaction between infiltration and seasonal water storage: there are no more dry impermeable soil layers. Seasonal LE and H fluxes in CLMgw have a more realistic variability (Figure 2b; green crosses) and R for hourly LE rises from 0.55 in CLM3.0 to 0.66 in CLMgw. It stays nearly constant for H (0.56 to 0.53). Although soil moisture in the upper 30 cm does not significantly increase (Figure 2a; green line), the new scheme has increased summer LE (Figure 2f; red and green lines) due to a higher soil moisture availability in lower depths (Figure 3b; CLMgw). But it also has increased off-season LE for the same reason (Figure 2e; red and green lines).

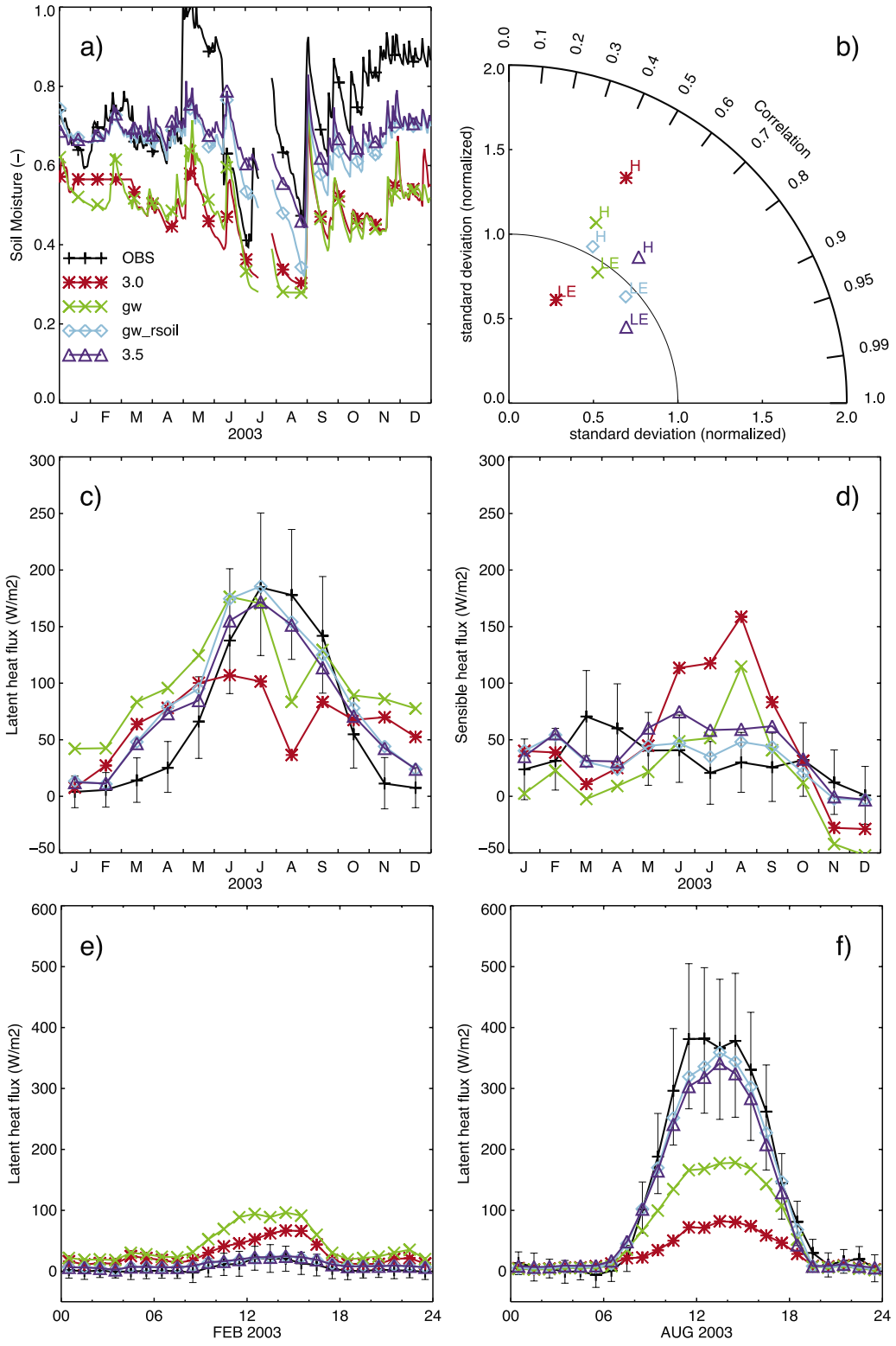

Figure 2. Model diagnostics at a temperate deciduous forest (Morgan Monroe State Forest, USA) during 2003: (a) soil moisture relative to saturation at 30 cm depth; (b) Taylor diagram with hourly statistics of LE and H fluxes; (c) monthly LE fluxes; (d) monthly H fluxes; (e) diurnal cycle of LE fluxes in February; (f) diurnal cycle of LE fluxes in August. Error bars show estimated uncertainties of observed turbulent fluxes. Legend: observations: black plus signs; CLM3.0: red asterisks; CLMgw: green crosses; CLMgw_rsoil: cyan diamonds; CLM3.5: violet triangles.

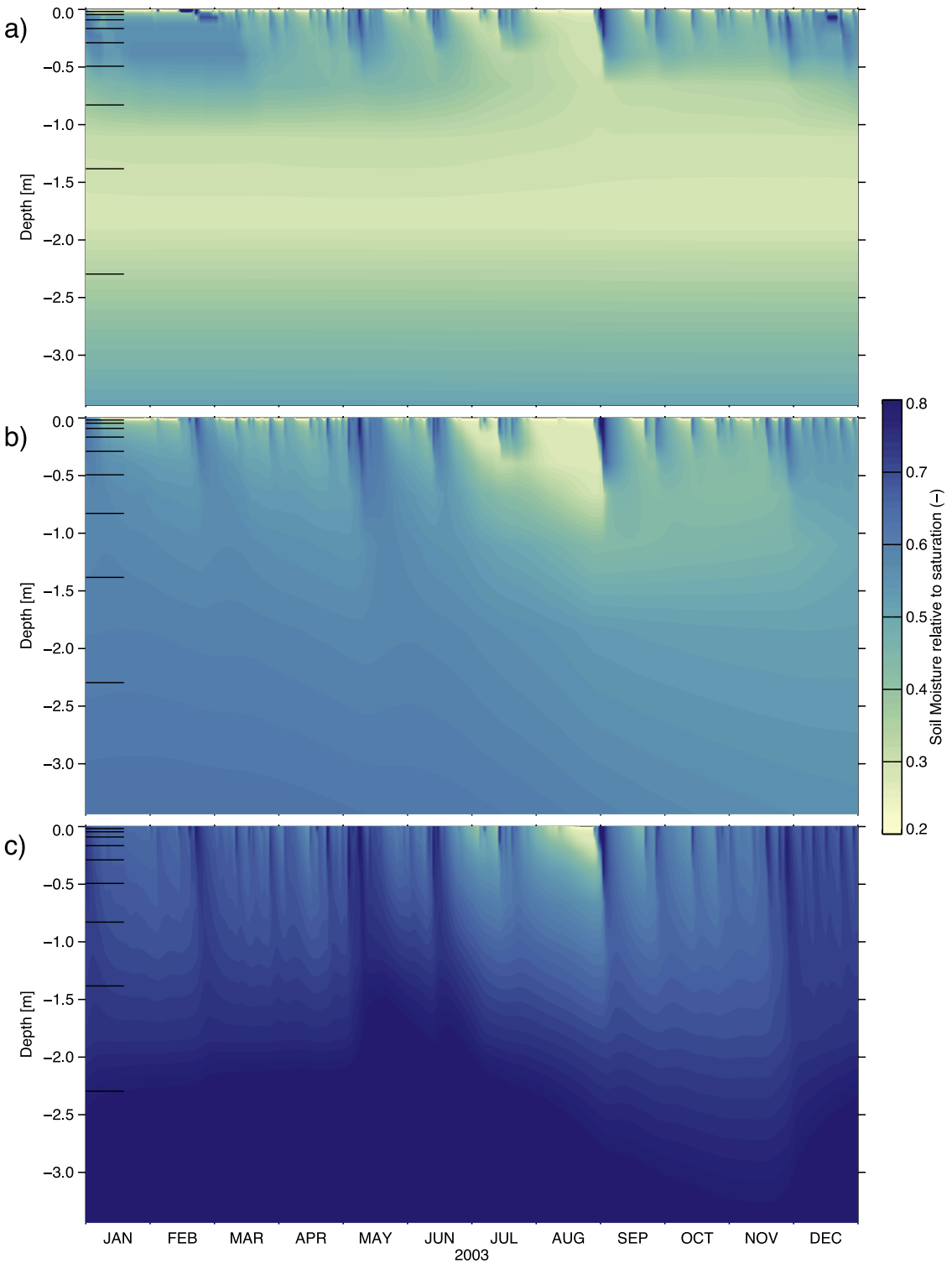

Figure 3. Simulated soil moisture profiles at a temperate deciduous forest (Morgan Monroe State Forest, USA) during 2003. Model versions: (a) CLM3.0; (b) CLMgw; (c) CLMgw_rsoil.

[37] The implementation of a more realistic soil water treatment reveals a deficiency of the model: given enough soil water and low leaf-coverage during off-season periods, CLMgw simulates excessive bare soil evaporation compared to observations. The same problem was present in CLM3.0 but it was mostly hidden by the generally dry soil conditions. Addition of the empirically derived bare soil resistance [*Sellers et al.*, 1992] offers a constraint for bare soil evaporation fluxes during periods of low leaf coverage in deciduous forests.

[38] It leads to a significant improvement of the simulated terrestrial water cycle in CLMgw_rsoil (Figure 3c): the water

table rises above the bottom of the soil water column and now displays dynamics within the biophysically active root zone. The root zone soil moisture is more comparable to observed values (Figure 2a; cyan line). Concurrently hourly and seasonal H and LE fluxes show a more realistic seasonal variability (Figures 2b–2f; cyan diamond symbols/lines). Aquifer water storage provides a mechanism for making winter and spring precipitation available as soil moisture during summer in order to sustain transpiration (Figure 2f, cyan line). R for hourly LE rises from 0.66 in CLMgw to 0.78 CLMgw_rsoil and for H it rises from 0.53 to 0.57 (Table 3). A similar improvement can be seen on the monthly timescale, where R of LE rises from 0.85 to 0.95 and RMSE is cut by around 30%. The remaining range of RMSE values on the order of 20–40 W m^{-2} is comparable to stochastic observation uncertainties (Table 2). Those illustrated changes in soil hydrology have a very similar impact on surface energy partitioning at other temperate forests like Vielsalm, Tharandt and Harvard Forest (not shown).

[39] The site-observed increase in H during March and April before leaf emergence cannot be reproduced by the model. It still simulates excessive LE during this time period, mostly from bare soil evaporation (not shown). The implementation of nitrogen limitation in the final model version CLM3.5 has a small effect on soil moisture and mostly affects energy partitioning during summer. It leads to higher correlations of LE and H with observed values (Figure 2b), with hourly R for LE and H increasing to 0.85 and 0.73, respectively. Compared to CLMgw_rsoil monthly R values do not improve but RMSE values for LE and H decrease by another 20–30%.

3.4. North Boreal

[40] North boreal wetlands like the Kaamanen tundra site in northern Finland are characterized by a generally low evaporative demand, a short growing season and a hydrological cycle which is dominated by snow and frozen soil physical processes [*Laurila et al.*, 2001].

[41] Surface heat and water fluxes in this climatic environment are less sensitive to the hydrological deficiencies in CLM3.0 (Figures 4a and 4b). Soil temperatures do not differ much between model versions (Figure 4c) and the annual cycle of soil temperature compares well to observed values which indicates that the snow cover duration and snow thermal properties are reasonably simulated at Kaamanen: 30 cm soil temperature remains roughly at freezing from January–April in 2004; during this period snow coverage and soil freezing processes are thermally decoupling the soil from the atmosphere. However, soil temperatures tend to be too warm during summer and too cold during the fall. This temperature bias may be due to the lack of an insulating organic soil layer in CLM. *Lawrence and Slater* [2008] suggest a method in which soil organic matter can be treated in CLM, which generally results in somewhat cooler summer soil temperatures. Hourly LE and H of CLM3.0 show R values of 0.71 and 0.76, respectively (Table 3 and Figures 4a and 4b), and only slightly improve/worsen to 0.88 and 0.74 in CLM3.5. Even though turbulent surface fluxes are insensitive to improvements in cold climate soil hydrology, changes in the whole terrestrial water cycle will now be analyzed. The 2004 snowmelt at Kaamanen serves as an example for the hydrological impacts of the new formulations in the simulations CLMgw and CLMgw_rsoil and CLM3.5.

[42] Modeled snowmelt at the end of April 2004 releases 250 mm of water (not shown) which can be distributed between the different terrestrial water storage (TWS) components: surface runoff, drainage runoff, soil water and evapotranspiration. Figure 4d summarizes the TWS as a function of storage change over time. A rise in TWS indicates water fluxes into the ecosystem (e.g., snow accumulation, soil water storage), negative directions are water losses from the ecosystem (transpiration, runoff). CLM3.0 loses around 250 mm of water at the time of snowmelt, concurrently with the increase in accumulated total runoff (Figure 4f). Both CLMgw and CLMgw_rsoil simulate accumulated snowmelt runoff on the order of 100–150 mm, much less than CLM3.0. The rest of the snowmelt water is kept in the ecosystem due to enhanced infiltration, the implementation of a fractional impermeable area and water storage physics of the new formulation. The soil resistance parameterization CLMgw_rsoil on top of CLMgw does not further affect TWS, and R values are mostly unchanged on both hourly and monthly timescale (Table 3). Excessive off-season soil evaporation is not a problem here, mainly because of snow coverage, frozen soils and a low atmospheric evaporative demand during these periods. A more stable calculation of the water table depth in CLM3.5 [see *Oleson et al.*, 2007, Appendix C] further creates a more gradual response of drainage runoff after snowmelt (Figure 4f; violet line). Surface runoff (Figure 4e) changes from CLM3.0 to CLMgw as a result of the enhanced infiltration formulation. While tower-scale runoff measurements are not available, *Oleson et al.* [2008] demonstrate that, indeed, the new model significantly improves arctic and boreal snowmelt runoff magnitude and phase.

3.5. Mediterranean

[43] The summer-dry mediterranean climate at Castelporziano (Italy) provides an important exercise for the new soil hydrology. As shown in detail for the temperate climate zone, CLM3.0 has severe shortcomings in simulating seasonal soil water storage. In Castelporziano summer drought generally lasts from June until October. Most of the yearly precipitation falls during winter and spring. Summer 2003 in Europe was exceptionally dry and hot [*Schär et al.*, 2004] with reduced evapotranspiration (resulting in a higher bowen ratio) and higher surface temperatures throughout the continent [*Zaitchik et al.*, 2006]. Castelporziano showed 47% less GPP and 3.5K higher air temperatures from Jul–Sep 2003 compared to 2002 [*Ciais et al.*, 2005].

[44] Figure 5b summarizes the performance of simulated LE and H at Castelporziano for the four model versions during the heat wave in 2003. During 2003 CLM3.0's R for hourly LE is quite low at 0.22, but increases to 0.37 for CLMgw, 0.77 for CLMgw_rsoil and 0.75 for CLM3.5 (Table 3 shows statistics for the full time period 2000–2005). R values for hourly and monthly H remain high for all model versions. Figure 5b shows that the new surface hydrology improves R for hourly LE and creates a more realistic variability for H. The surface energy balance at

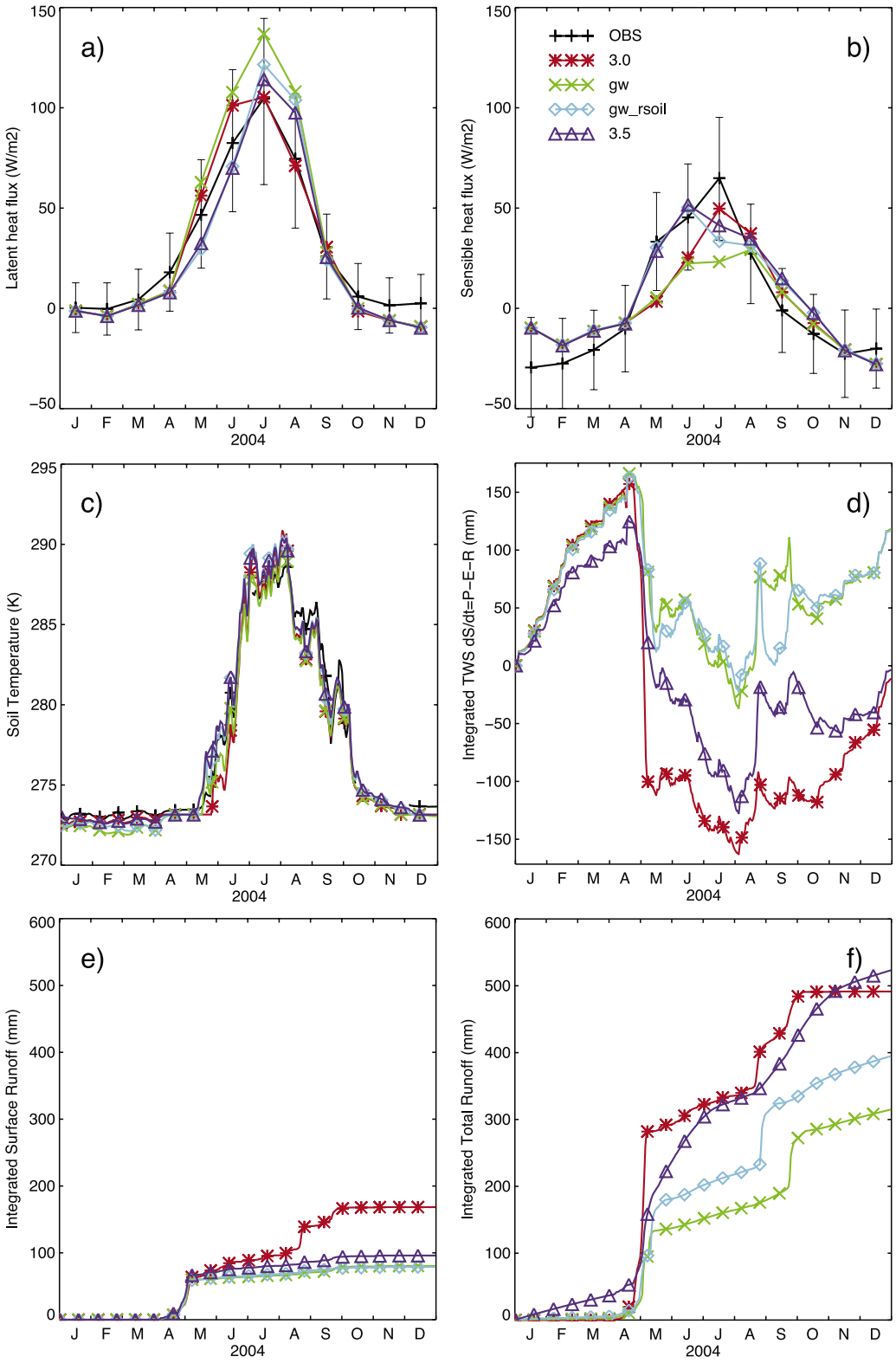

Figure 4. Model diagnostics at a north boreal tundra ecosystem (Kaamanen, Finland) during 2004: (a) monthly LE fluxes; (b) monthly H fluxes; (c) soil temperature at 30 cm; (d) terrestrial water storage; (e) accumulated surface runoff; (f) accumulated total runoff. Error bars show estimated uncertainties of observed turbulent fluxes. Legend: observations: black plus signs; CLM3.0: red asterisks; CLMgw: green crosses; CLMgw_rsoil: cyan diamonds; CLM3.5: violet triangles.

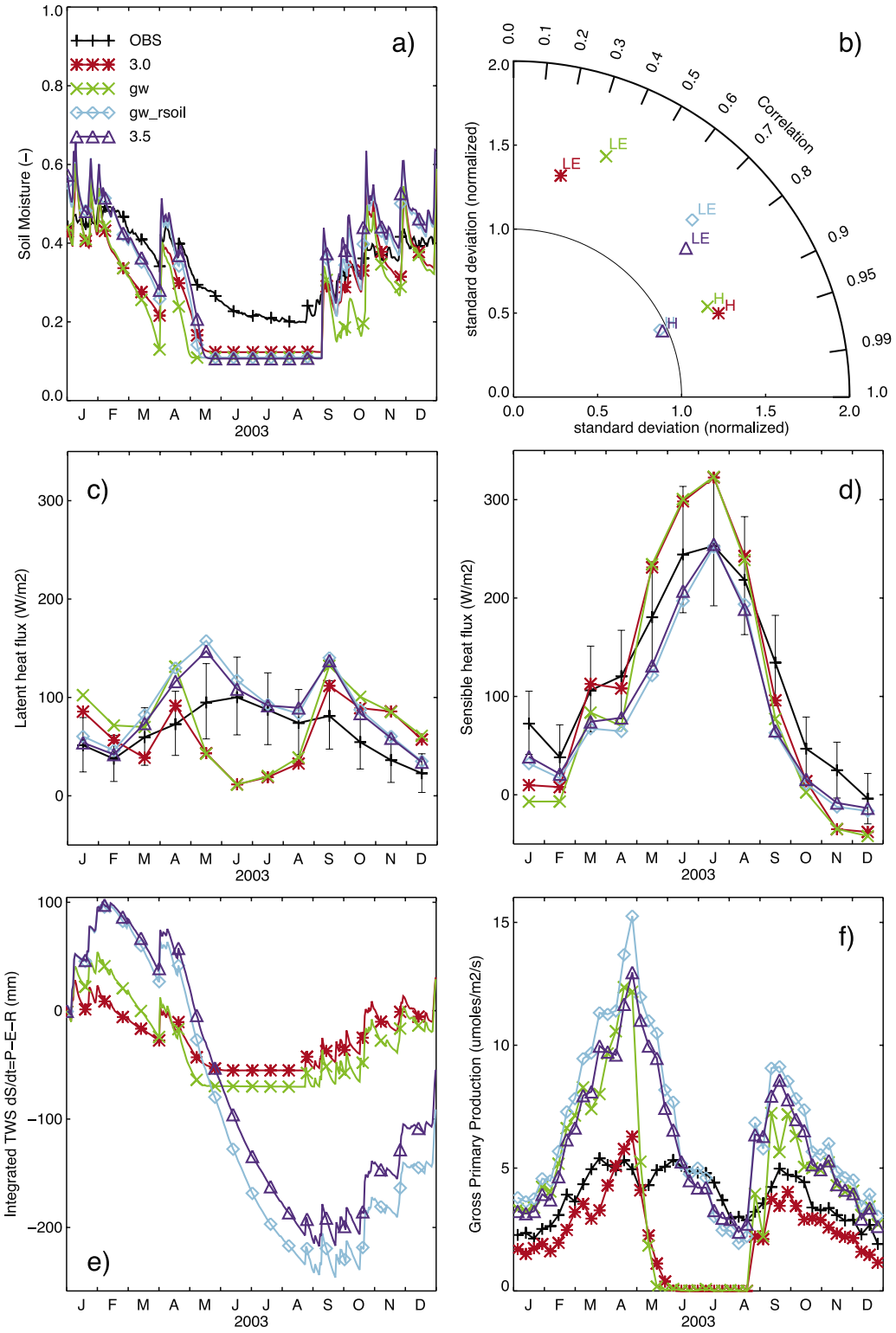

Figure 5. Model diagnostics at a mediterranean hardwood forest (Castel Porziano, Italy) for 2003: (a) soil moisture at 30 cm depth; (b) Taylor diagram showing statistics from hourly LE and H fluxes; (c) monthly LE fluxes; (d) monthly H fluxes; (e) terrestrial water storage; (f) modeled versus NEE-derived GPP. Error bars show estimated uncertainties of observed turbulent fluxes. Legend: observations: black plus signs; CLM3.0: red asterisks; CLMgw: green crosses; CLMgw_rsoil: cyan diamonds; CLM3.5: violet triangles.

Castelporziano is dominated by H. In comparison to a more humid ecosystem, improving LE at a dry ecosystem only has a small effect on the diurnal course of H. However, as can be seen in Figure 5b, a better simulation of LE can shift the absolute magnitude and therefore seasonal variability of H towards observed values.

[45] CLM3.0 simulates a low magnitude and damped seasonal course of soil moisture compared to observed soil moisture at 30 cm depth (Figure 5a). It coincides with a low simulated TWS magnitude (the range between the minimum and the maximum TWS during a year) of around 60 mm (Figure 5e). Concurrently LE is almost completely absent in the summer months from May to August (Figure 5c), resulting in a too high H during this time period (Figure 5d). This result explains the exaggerated variability and low correlation of CLM3.0 and CLMgw displayed in Figure 5b. While the addition of groundwater storage (CLMgw) rises TWS magnitude to 120 mm, it cannot overcome the unrealistic drought stress during summer months. The bare soil resistance constrains off-season evaporation losses (Figure 5c; CLMgw_rsoil) and augments TWS magnitude to over 300 mm. The soil water storage capability of the groundwater scheme becomes effective when the soil model's numerics and physics show a more stable interaction.

[46] The new hydrology of CLMgw_rsoil is able to supply the extensive water demand at this ecosystem during the dry summer 2003. A storage deficit of around 100 mm persists into the next year (Figure 5e). Although the off-season observed soil moisture levels correspond well to those modeled in CLMgw_rsoil, the model's soil at 30 cm still dries out too much during summer. Deeper soil levels act as the large TWS buffer in this case. *Reichstein et al.* [2003] notes that the site's vegetation has access to topographically induced groundwater (lateral groundwater recharge), which was not simulated here.

[47] Similarly to LE, modeled GPP (Figure 5f) becomes more realistic from CLM3.0 to CLMgw_rsoil during summer. But GPP and LE are now overestimated during other parts of the year. The new sun-shade canopy scheme implemented by *Thornton and Zimmermann* [2007] has a more realistic light interception parameterization for canopy-integrated photosynthesis but depends on the quantification of nitrogen as a controlling factor for this process. The standard model does not include nitrogen controls on photosynthesis. After soil hydrology is fixed in CLMgw_rsoil we now find that GPP is overestimated. PFT-dependent V_{max} scaling factors $f(N)$ simulating nitrogen limitation are presented in *Oleson et al.* [2007] and applied in CLM3.5. As a result of the decreased light response (Figure 5f, violet triangles), GPP and LE slightly decrease during spring and autumn. However, this newly introduced formulation alone cannot account for the exaggerated fluxes. GPP (and to a lesser extent also LE) is still highly overestimated during the wet season.

3.6. Tropical

[48] The evergreen tropical broadleaf forest site KM83 south of Santarem (Brazil) represents a constant hot and humid climate [*da Rocha et al.*, 2004]. 70% of the annual precipitation occur within the seven month long wet season from January to July.

[49] Figures 6c and 6d show that accumulated LE and H fluxes are simulated accurately during the wet season with CLM3.0, but the observed continuous increase in accumulated water flux throughout the dry season from August to December cannot be sustained, resulting in a very high bowen ratio during this latter period. CLMgw, CLMgw_rsoil and CLM3.5 provide remedy for this deficiency: R for hourly LE steadily increases from 0.52 to 0.76 (Table 3). R for hourly H decreases from 0.59 to 0.41 for CLMgw and increases again to 0.68 for CLM3.5. The generally low H at this site (within the uncertainty range of observations) renders the correlation coefficient as an unsuitable measure for performance comparisons (this is even more evident at the other tropical site KM67). RMSE is a more robust measure. On the hourly timescale it decreases significantly from 166.1 W m^{-2} to 92.0 W m^{-2}.

[50] Little difference is found between the aquifer water storage formulation only (CLMgw) and the use of an additional bare soil evaporation resistance formulation (CLMgw_rsoil). For instance, R for LE rises from 0.74 to 0.77 on the hourly timescale. Constant and high leaf coverage at this site provides a radiation-driven process for the control of excessive bare soil evaporation, so the addition of the missing resistance term is not critical for this evergreen tropical ecosystem.

[51] A comparison between modeled and measured soil moisture at 20 cm depth in Figure 6a does not provide much evidence for why dry season LE is enhanced in CLMgw_rsoil compared to CLM3.0; most of the model enhancements seem to influence lower soil depths. There were no soil moisture measurements reported for depths below 1 m. The modeled TWS cycle in Figure 6b provides insight into the relevant hydrological processes: while CLM3.0 has a very low TWS magnitude of less than 100 mm, CLMgw and CLMgw_rsoil push TWS magnitude to 400 mm. Seasonal soil water storage with such a high capacity is important for a tropical ecosystem since plant biophysical functioning in a seasonally dry climate depends on long-term soil moisture dynamics. This is supported by observational evidence: *da Rocha et al.* [2004] show that the Amazonian rainforest at KM83 can sustain transpiration throughout the dry season since it has access to deep soil water.

[52] As already shown for the mediterranean site, CLMgw_rsoil with the more realistic soil water cycle leads to overestimated LE and GPP. Including the parametric nitrogen limitation $f(N)$ in CLM3.5 results in a more realistic LE and H balance for both wet and dry season (Figures 6c and 6d). R for hourly LE remains roughly constant (0.76, compared to 0.77 for CLMgw_rsoil), but RMSE is reduced by around 15 W m^{-2}. On the other hand, R for hourly H significantly increases from 0.39 to 0.68 and RMSE is reduced by 26 W m^{-2}. GPP is still overestimated during the wet season. However, a slightly more realistic light response of GPP (Figures 6e and 6f) is achieved. In a high light environment such as the Amazon, stomatal conductance during daylight is mostly constrained by the maximum rate of carboxylation. The factor $f(N)$ has the largest absolute effects on GPP for these ecosystems. LE (and thus the surface energy partitioning) is influenced to a lesser extent, as LE is also controlled by the boundary layer

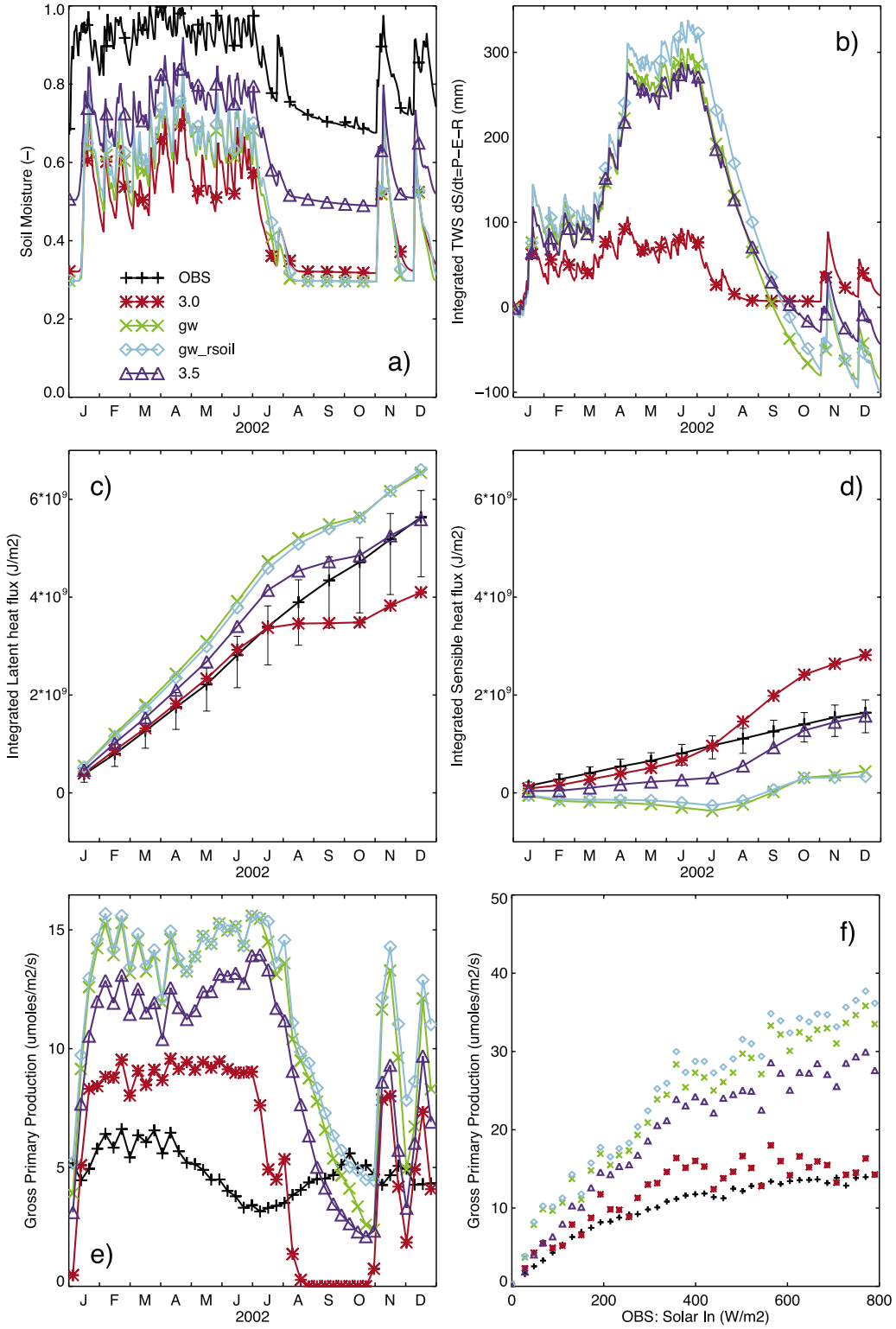

Figure 6. Model diagnostics at a tropical evergreen forest (Santarem KM83, Brazil) during 2002: (a) soil moisture at 20 cm depth; (b) terrestrial water storage; (c) accumulated LE fluxes; (d) accumulated H fluxes; (e) modeled versus NEE-derived GPP; (f) mean light response curves for modeled and NEE-derived GPP (binned by incoming solar radiation). Error bars show estimated uncertainties of observed turbulent fluxes. Legend: observations: black plus signs; CLM3.0: red asterisks; CLMgw: green crosses; CLMgw_rsoil: cyan diamonds; CLM3.5: violet triangles.

vapor pressure gradient, bare soil evaporation and aerodynamical properties.

4. Discussion

[53] Turbulent heat and water fluxes of the original CLM3.0 show significant biases in tropical, mediterranean and temperate climatic environments. These biases result from a poor representation of soil moisture storage and its interaction with seasonal variations of the surface climate. Modeled plant transpiration generally shuts down during either summer or dry seasons due to a lack of soil moisture supply. Observations from the 15 flux tower sites, however, indicate that plants can sustain their physiological function during seasonal-scale and longer term drought periods. Subsurface hydrological processes on which these plants largely depend therefore need to be properly represented in land surface models in order to simulate the terrestrial carbon and water cycle [*Reichstein et al.*, 2002]. This requirement gains further importance in view of the predicted temperature and precipitation changes in future climate scenarios, which could severely affect ecosystem function during hotter and drier summer periods [*Seneviratne et al.*, 2006].

4.1. Terrestrial Water Storage

[54] To achieve a higher water storage capacity in a land surface model, the total soil depth and other soil parameters are often modified as a first guess. The above findings, however, suggest that soil water storage capacity is a dynamic quantity. It does not primarily depend on soil physical parameters. It rather results from a consistent interplay between the soil and vegetation biophysical parameterizations on one side and the soil numerical scheme on the other side: they both depend on each other in order to provide a realistic simulation of the terrestrial water cycle.

[55] At the mediterranean and temperate sites only small improvements in surface fluxes result from the implementation of larger soil water storage capacity by use of a prognostic aquifer scheme. Soil water infiltration and storage are both still largely inhibited by excessive bare soil evaporation during off-season periods in those ecosystems. Further addition of a bare soil evaporation resistance finally results in a realistic TWS magnitude and concurrently in a substantial increase of turbulent flux R and decrease in RMSE at most sites. Figures 3a–3c illustrate the underlying soil hydrological processes:

[56] 1. A dry soil can continuously inhibit vertical soil moisture fluxes and thus decrease seasonal water storage by hydrologically decoupling upper from lower soil layers.

[57] 2. Extending the storage pool by implementing a prognostic aquifer breaks the infiltration barrier by providing ample soil moisture to the root zone but TWS remains at a low seasonal magnitude (e.g., Figure 5e).

[58] 3. Bare soil evaporation during off-season periods was identified as the main process which dampens TWS magnitude for deciduous vegetation in temperate and mediterranean climate zones. With a more realistic off-season bare soil evaporation TWS becomes positive during the winter or wet season when moisture is stored in the soil. As a consequence transpiration fluxes during months of low rainfall (dry season) or large atmospheric demands (summer season) substantially improve.

[59] While a prognostic aquifer model [*Niu et al.*, 2005, 2007] provides the physical framework for simulating large seasonal TWS fluctuations, the size of TWS magnitude depends on a dynamically varying set of involved soil and vegetation processes. The new hydrological formulations enhance TWS by 200–300 mm compared to the original CLM3.0, with quite beneficial effects for the simulated surface energy and water balances in seasonally dry climates. This result is highly consistent with comparisons between modeled and GRACE estimates of TWS at catchment scale presented by *Oleson et al.* [2008]. They show that CLM3.5 enhances TWS magnitude by 50–300 mm compared to CLM3.0, with improved correlations and substantial decreases in RMSE.

[60] In northern boreal regions like Kaamanen, however, TWS magnitude decreases by around 100 mm when groundwater storage is added (Figure 4e). This behavior is opposite to what one would expect. As in warm climates, soil water storage function of cold climates not only depends on storage capacity, but closely interacts with the dominant hydrological processes through time-delayed feedbacks: the analysis shows that snowmelt water can be stored in spring after soil thaw and should not completely run off into rivers like in the original formulation. Soil moisture storage seems to dampen the seasonal course of TWS at Kaamanen. While adding groundwater does not much affect turbulent surface fluxes in cold climates (Figures 4a and 4b) it could lead to improvements in high latitude runoff timing and magnitude (Figures 4e and 4f). This is documented in *Oleson et al.* [2008] by comparison of global simulated versus observed river discharge and runoff.

4.2. Nitrogen Limitation

[61] Results from the mediterranean and tropical sites suggest that the enhanced and more realistic water storage processes in the model can lead to excessive transpiration. The addition of a parameterized nitrogen control for photosynthesis decreases light sensitivity of stomatal opening as expected (Figures 5f, 6e, and 6f). The need for this parameterization only became evident after the new soil hydrology and the new canopy integration scheme was implemented: maximum photosynthesis rates in CLM3.0 were fixed, based on observed values. Low soil moisture levels furthermore limited the plant physiological activity in most climates. Parameterized nitrogen control became a necessity with the new hydrological modifications. While nitrogen is an important controlling factor for most terrestrial ecosystems ($f(N)$ ranging from 0.60–0.84 in *Oleson et al.* [2007]), our results suggest that it mostly affects the surface energy and water balance in environments with high GPP. Tropical broadleaf forests have the lowest diagnosed nitrogen limitations among the 16 PFTs (highest $f(N)$ = 0.84). However, they mostly operate at high light levels, resulting in the largest nitrogen-controlled decreases in GPP in absolute terms. In comparison to GPP, LE is less sensitive to changes in stomatal conductance through nitrogen control because LE is a composite of transpiration and bare soil evaporation. The latter is independent of nitrogen availability. LE is further controlled by boundary layer aerodynamical

resistances, which only indirectly and weakly influence GPP. Nevertheless, results show a positive effect of the newly introduced $f(N)$ on R and RMSE of hourly and monthly LE and H fluxes. The two tropical sites KM67 and KM83 show the largest decrease in RMSE (Table 3) by including $f(N)$ compared to simulations with changes in soil hydrology alone. Boundary layer processes for these ecosystems are expected to benefit from this model enhancement in coupled simulations.

4.3. Open Questions

[62] Figures 5f and 6f show that yet another process might be missing. LE and GPP are still overestimated during the wet season at the mediterranean and the tropical site. LE is less of a problem than GPP since LE is also driven by the atmospheric vapor pressure gradient and surface layer aerodynamics. It furthermore is composited from plant transpiration and bare soil evaporation, the latter being unrelated to stomatal functioning. Suggestions for missing processes are, e.g., a prognostic dry season phenology (which can also vary in tropical ecosystems [*Myneni et al.*, 2007]) and dynamic allocation of leaf structure and photosynthates [*Dickinson et al.*, 2002], which are not simulated in the standard CLM. Simulations for mediterranean and tropical FLUXNET sites employing CLM3.5 with its full biogeochemistry scheme [*Thornton et al.*, 2007] could shed some light into these open questions. Figures 2c and 2d show that CLM3.5 still cannot represent the H peak during March and April just before leaf emergence in temperate forests. This problem is common to many land surface models and might be related to model deficiencies in either phenology (too early leaf emergence) or surface litter cover (too much bare soil evaporation) and should be addressed in future studies.

5. Conclusion

[63] The Community Land Model version 3 includes mechanistic representations of terrestrial radiation, heat, water and carbon exchange processes, which have been developed from laboratory experiments and field studies. Deficiencies in the CLM3.0 soil hydrology have been revealed from long-term climate simulations, with sometimes negative effects on surface climate and plant biogeography. In this study new algorithms for removing these deficiencies were tested in off-line simulations at 15 FLUXNET tower sites.

[64] 1. The prognostic aquifer scheme [*Niu et al.*, 2007] extends the soil storage pool of CLM3.0, but this enhancement only becomes effective when bare soil evaporation is curtailed by the application of an empirical bare soil resistance term [*Sellers et al.*, 1992]. Soil water storage in models like CLM strongly depends on the interplay between soil numerics (nonlinear state-parameter dependence) and terrestrial biophysics. In this case excessive off-season bare soil evaporation in deciduous ecosystems inhibited groundwater storage by successively reducing long term soil moisture levels below a threshold at which hydraulic conductivity allows for vertical water transfer in the finite difference soil water scheme.

[65] 2. As a consequence of these two enhancements, CLM3.5 now includes a more dynamic soil water storage capacity: TWS magnitude increases in tropical, mediterranean and temperate climates and decreases in cold climates. This result was mainly achieved by introduction of mechanistic hydrological processes and neither by extending the soil depth nor by modifying soil hydraulic parameters. In support of this conclusion [*Gulden et al.*, 2007] find that a model with a prognostic aquifer is less sensitive to the largely unknown and spatially variable set of soil hydraulic parameters compared to a model with a deep soil alone. The uncertainty in the prescription of soil physical parameters in land surface models should therefore be mitigated by use of more mechanistic formulations for soil water storage. Furthermore this result justifies and facilitates comparisons between tower sites with similar vegetation but different soils.

[66] 3. Nitrogen control of photosynthesis (and therefore stomatal opening and transpiration) is needed in order to correctly partition energy into turbulent heat and water fluxes in environments with high GPP. This missing process was only uncovered after soil hydrological modifications led to a better simulated subsurface water balance and the new canopy integration scheme created a more realistic light response of photosynthesis. The original CLM3.0 was providing the right results for the wrong reasons: stomates in tropical and mediterranean ecosystems were seasonally closing due to missing water supply while observations indicate that photosynthesis in those ecosystems is not so sensitive to drought effects.

[67] 4. Despite above improvements CLM3.5 still overestimates GPP during the wet season in mediterranean and tropical ecosystems. Although the surface energy partitioning is less sensitive to stomatal response than GPP, we hypothesize that drought phenology or biogeochemical feedbacks involving the full terrestrial carbon-nitrogen cycle could be responsible for these differences. Local-scale and species-specific soil and vegetation properties and furthermore the general underestimation of eddy covariance fluxes might explain some differences between observed and modeled turbulent fluxes [*Wilson et al.*, 2002; *Foken et al.*, 2006]. The steady reduction of RMSE into the range of observation uncertainty (or below; e.g., for monthly fluxes at Kaamanen: RMSE = 10–20 W m^{-2}) in boreal, northern boreal and temperate climates as a result of the new mechanistic formulations is a strong indicator for the success of CLM's new hydrology. In seasonally dry and tropical climates most uncertainty may still be on the model's side, since monthly RMSE ranges between 30–50 W m^{-2}), which is larger than estimated errors in observations.

[68] 5. A land surface model should as a first step include a realistic set of mechanistic formulations, which was the focus of this study. This leads to a better understanding of the role of ecophysiological drivers such as water, light and nitrogen in controlling photosynthesis at a range of ecosystems, and it thus helps to either support or invalidate some of our above hypotheses. It further makes the model suitable for global predictive applications across a range of spatial and timescales. As noted by *Abramowitz* [2005], there are, however, still considerable opportunities for improvements in such models. In a second step, the many empirical model parameters should be constrained in order to further reduce model uncertainty. The currently developed standardized,

gap-filled and bias-corrected FLUXNET Synthesis data set involving more than 200 tower sites (D. Papale and M. Reichstein, personal communication, 2007) provides a global set of observations suitable for a data assimilation exercise aimed at reducing parameter uncertainty in land surface models.

[69] While at first the small number of 15 FLUXNET towers seems to be inappropriate for testing a globally applicable land surface model, we demonstrate that focusing on only four sites already effectively helps to identify and correct for major missing soil hydrological and vegetation biophysical processes in the model. As already shown by *Stöckli and Vidale* [2005], such a modeling framework with offline simulations allows for computationally inexpensive research and development of land surface models. FLUXNET provides valuable observations of quantities at timescales which are relevant in climate simulations. Despite lacking global coverage, FLUXNET statistically inherits the whole global set of ecosystems and climate zones. Although individual sites differ in absolute magnitude and timing of heat, water and carbon fluxes, they show similar patterns for sites within certain ecosystem and climate zones. Similarly, model deficiencies become visible as consistent patterns of time and phase shifts on diurnal and seasonal timescales across a number of sites, which was demonstrated here. While this study explored hourly-seasonal terrestrial processes, there is an increased number of FLUXNET sites with 10 years or longer coverage which allow a similar analysis for the interannual timescale.

[70] *Oleson et al.* [2008] further shows that, indeed, those identified and corrected processes at local scale are applicable to the global scale and lead to improvements in the simulation of the terrestrial water cycle. This might be a step towards an answer in the debate on land-atmosphere coupling strength [*Koster et al.*, 2006; *Guo et al.*, 2006]. *Dirmeyer et al.* [2006] find that turbulent surface fluxes and planetary boundary layer processes still respond very differently to soil moisture states among models. However, models should be able to reproduce the basic relationships in land-atmosphere interactions found in observational-based analysis data sets [*Betts*, 2004]. A more realistic seasonal-interannual hydrology in a land surface model is also a prerequisite for the functioning of dynamic vegetation [*Bonan and Levis*, 2006] and biogeochemical model components [*Thornton et al.*, 2007].

[71] The new and publicly available Community Land Model CLM3.5 includes all the above improvements. Its application within the Community Climate System Model should have beneficial impacts on the simulated global carbon and water cycle.

[72] **Acknowledgments.** We acknowledge the NASA Energy and Water Cycle Study (NEWS) grant NNG06CG42G as the main funding source of this study. We acknowledge the coordinating efforts by the CarboEurope IP, AmeriFlux and LBA projects as part of FLUXNET. Meteorological driver and validation data have been collected and prepared by the individual site PIs and their teams. We would like to thank Marc Aubinet (Vielsalm), Christian Bernhofer (Tharandt), Riccardo Valentini (Castelporziano and Collelongo), Tuomas Laurila (Kaamanen), Timo Vesala (Hyytiälä), Maria Jose Sanz (El Saler), Mike Goulden (Santarem KM83), Steven Wofsy (Santarem Km67 and BOREAS NSA Old Black Spruce), Hans Peter Schmid (Morgan Monroe State Forest), Brian Amiro (BOREAS NSA Old Black Spruce), Lawrence Flanagan (Lethbridge), Tilden Meyers (Fort Peck), Bill Munger (Harvard Forest) and Russ Monson (Niwot Ridge) for contributing data to this study.

References

Abramowitz, G. (2005), Towards a benchmark for land surface models, *Geophys. Res. Lett.*, *32*, L22702, doi:10.1029/2005GL024419.

Aubinet, M., B. Chermanne, M. Vandenhaute, B. Longdoz, M. Yernaux, and E. Laitat (2001), Long term carbon dioxide exchange above a mixed forest in the Belgian ardennes, *Agric. For. Meteorol.*, *108*(4), 293–315.

Baldocchi, D., et al. (2001), FLUXNET: A new tool to study the temporal and spatial variability of ecosystem-scale carbon dioxide, water vapor, and energy flux densities, *Bull. Am. Meteorol. Soc.*, *82*(11), 2415–2433.

Betts, A. K. (2004), Understanding hydrometeorology using global models, *Bull. Am. Meteorol. Soc.*, *85*, 1673–1688.

Betts, A. K., R. L. Desjardins, and D. Worth (2007), Impact of agriculture, forest and cloud feedback on the surface energy budget in boreas, *Agric. For. Meteorol.*, *142*(2–4), 156–169.

Betts, R. A., P. M. Cox, and F. I. Woodward (2000), Simulated responses of potential vegetation to doubled-CO_2 climate change and feedbacks on near-surface temperature, *Global Ecol. Biogeogr.*, *9*, 171–180.

Beven, K. J., and M. J. Kirkby (1979), A physically based, variable contributing area model of basin hydrology, *Hydrol. Sci. Bull.*, *24*(1), 43–69.

Bogena, H., K. Schulz, and H. Vereecken (2006), Towards a network of observatories in terrestrial environmental research, *Adv. Geosci.*, *9*, 109–114.

Bonan, G. B., and S. Levis (2006), Evaluating aspects of the community land and atmosphere models (CLM3 and CAM3) using a Dynamic Global Vegetation model, *J. Clim.*, *19*(11), 2290–2301.

Canadell, J. G., et al. (2000), Carbon metabolism of the terrestrial biosphere: A multitechnique approach for improved understanding, *Ecosystems*, *3*, 115–130.

Chen, J., and P. Kumar (2001), Topographic influence on the seasonal and interannual variation of water and energy balance of basins in North America, *J. Clim.*, *14*(9), 1989–2014.

Chen, T. H., et al. (1997), Cabauw experimental results from the project for intercomparison of land-surface parameterization schemes, *J. Clim.*, *10*, 1194–1215.

Ciais, P., et al. (2005), Europe-wide reduction in primary productivity caused by the heat and drought in 2003, *Nature*, *437*, 529–533.

Collins, W. D., et al. (2006), The Community Climate System Model version 3 (ccsm3), *J. Clim.*, *19*(11), 2122–2143.

Cox, P. M., R. A. Betts, C. D. Jones, S. A. Spall, and I. J. Totterdell (2000), Acceleration of global warming due to carbon-cycle feedbacks in a coupled climate model, *Nature*, *408*, 184–187.

da Rocha, H. R., M. L. Goulden, S. D. Miller, M. C. Menton, L. D. V. O. Pinto, H. C. de Freitas, and A. M. E. S. Figueira (2004), Seasonality of water and heat fluxes over a tropical forest in eastern amazonia, *Ecol. Appl.*, *14*(4), 22–32.

Desai, A. R., P. V. Bolstad, B. D. Cook, K. J. Davis, and E. V. Carey (2005), Comparing net ecosystem exchange of carbon dioxide between an old-growth and mature forest in the upper Midwest, USA, *Agric. For. Meteorol.*, *128*(1–2), 33–55.

Dickinson, R. E., et al. (2002), Nitrogen controls on climate model evapotranspiration, *J. Clim.*, *15*, 278–295.

Dickinson, R. E., K. W. Oleson, G. Bonan, F. Hoffman, P. Thornton, M. Vertenstein, Z. L. Yang, and X. B. Zeng (2006), The Community Land Model and its climate statistics as a component of the Community Climate System model, *J. Clim.*, *19*(11), 2302–2324.

Dirmeyer, P. A., R. D. Koster, and Z. C. Guo (2006), Do global models properly represent the feedback between land and atmosphere?, *J. Hydrometeorol.*, *7*(6), 1177–1198.

Dunn, A. L., C. C. Barford, S. C. Wofsy, M. L. Goulden, and B. C. Daube (2007), A long-term record of carbon exchange in a boreal black spruce forest: means, responses to interannual variability, and decadal trends, *Global Change Biol.*, *13*(3), 577–590.

Falge, E., et al. (2001), Gap filling strategies for long term energy flux data sets, *Agric. For. Meteorol.*, *107*, 71–77.

Flanagan, L. B., L. A. Wever, and P. J. Carlson (2002), Seasonal and interannual variation in carbon dioxide exchange and carbon balance in a northern temperate grassland, *Global Change Biol.*, *8*, 599–615.

Foken, T. (2008), The energy balance closure problem - an overview, *Ecol. Appl.*, in press.

Foken, T., F. Wimmer, M. Mauder, C. Thomas, and C. Liebethal (2006), Some aspects of the energy balance closure problem, *Atmos. Chem. Phys.*, *6*, 4395–4402.

Friedlingstein, P., J. L. Dufresne, P. M. Cox, and P. Rayner (2003), How positive is the feedback between climate change and the carbon cycle?, *Tellus, Ser. B*, *55*(2), 692–700.

Friedlingstein, P., et al. (2006), Climate-carbon cycle feedback analysis: Results from the (CMIP)-M-4 model intercomparison, *J. Clim.*, *19*(14), 3337–3353.

Friend, A. D., et al. (2007), FLUXNET and modelling the global carbon cycle, *Global Change Biol.*, *13*, 610–633.

Gabathuler, M., C. A. Marty, and K. W. Hanselmann (2001), Parameterization of incoming longwave radiation in high-mountain environments, *Phys. Geogr.*, *22*(2), 99–114.

Gedney, N., P. M. Cox, H. Douville, J. Polcher, and P. J. Valdes (2000), Characterizing GCM land surface schemes to understand their responses to climate change, *J. Clim.*, *13*, 3066–3079.

Gilmanov, T. G., L. L. Tieszen, B. K. Wylie, L. B. Flanagan, A. B. Frank, M. R. Haferkamp, T. P. Meyers, and J. A. Morgan (2005), Integration of CO_2 flux and remotely-sensed data for primary production and ecosystem respiration analyses in the northern Great Plains: potential for quantitative spatial extrapolation, *Global Ecol. Biogeogr.*, *14*(3), 271–292.

Goulden, M. L., S. D. Miller, H. R. da Rocha, M. C. Menton, H. C. de Freita, A. M. E. S. Figueira, and C. A. D. de Sousa (2004), Diel and seasonal patterns of tropical forest CO_2 exchange, *Ecol. Appl.*, *14*(4), 42–54.

Grunwald, T., and C. Bernhofer (2007), A decade of carbon, water and energy flux measurements of an old spruce forest at the anchor station Tharandt, *Tellus, Ser. B*, *59*, 387–396.

Gulden, L. E., E. Rosero, Z. L. Yang, M. Rodell, C. S. Jackson, G. Y. Niu, P. J. F. Yeh, and J. Famiglietti (2007), Improving land-surface model hydrology: Is an explicit aquifer model better than a deeper soil profile?, *Geophys. Res. Lett.*, *34*, L09402, doi:10.1029/2007GL029804.

Guo, Z. C., et al. (2006), Glace: The Global Land-Atmosphere Coupling Experiment. Part II: analysis, *J. Hydrometeorol.*, *7*(4), 611–625.

Hack, J. J., J. M. Caron, S. G. Yeager, K. W. Oleson, M. M. Holland, J. E. Truesdale, and P. J. Rasch (2006), Simulation of the global hydrological cycle in the CCSM Community Atmosphere Model version 3 (CAM3): Mean features, *J. Clim.*, *19*(11), 2199–2221.

Henderson-Sellers, A., K. McGuffie, and A. J. Pitman (1996), The Project for Intercomparison of Land-surface Parametrization Schemes (PILPS): 1992 to 1995, *Clim. Dyn.*, *12*, 849–859.

Henderson-Sellers, A., P. Irannejad, K. McGuffie, and A. J. Pitman (2003), Predicting land-surface climates - better skill or moving targets?, *Geophys. Res. Lett.*, *30*(14), 1777, doi:10.1029/2003GL017387.

Hollinger, D. Y., and A. D. Richardson (2005), Uncertainty in eddy covariance measurements and its application to physiological models, *Tree Physiol.*, *25*(7), 873–885.

Hutyra, L., J. W. Munger, S. R. Saleska, E. W. Gottlieb, B. C. Daube, A. L. Dunn, D. F. Amaral, P. B. de Camargo, and S. C. Wofsy (2007), Seasonal controls on the exchange of carbon and water in an Amazonian rain forest, *J. Geophys. Res.*, *112*, G03008, doi:10.1029/2006JG000365.

Idso, S. B. (1981), A set of equations for full spectrum and 8-mu-m to 14-mu-m and 10.5-mu-m to 12.5-mu-m thermal-radiation from cloudless skies, *Water Resour. Res.*, *17*, 295–304.

Koster, R. D., et al. (2004), Regions of strong coupling between soil moisture and precipitation, *Science*, *305*, 1138–1140.

Koster, R. D., et al. (2006), Glace: The Global Land-Atmosphere Coupling Experiment. Part I: overview, *J. Hydrometeorol.*, *7*(4), 590–610.

Laurila, T., H. Soegaard, C. R. Lloyd, M. Aurela, J. P. Tuovinen, and C. Nordstroem (2001), Seasonal variations of net CO_2 exchange in European Arctic ecosystems, *Theor. Appl. Climatol.*, *70*(1–4), 183–201.

Lawrence, D. M., and A. G. Slater (2008), Incorporating organic soil into a global climate model, *Clim. Dyn.*, doi:10.1007/s00382-007-0278-1, in press.

Lawrence, D. M., P. E. Thornton, K. W. Oleson, and G. B. Bonan (2007), The partitioning of evapotranspiration into transpiration, soil evaporation, and canopy evaporation in a gcm: Impacts on land-atmosphere interaction, *J. Hydrometeorol.*, *8*, 862–880.

Levis, S., G. B. Bonan, M. Vertenstein, and K. W. Oleson (2004), The community land model's dynamic global vegetation model (clm-dgvm): Technical description and user's guide, *NCAR Tech. Note TN-459+IA*, Natl. Cent. for Atmos. Res., Boulder, Colo.

Monson, R. K., A. A. Turnipseed, J. P. Sparks, P. C. Harley, L. E. Scott-Denton, K. Sparks, and T. E. Huxman (2002), Carbon sequestration in a high-elevation, subalpine forest, *Global Change Biol.*, *8*(5), 459–478.

Myneni, R. B., et al. (2007), Large seasonal swings in leaf area of Amazon rainforests, *Proc. Natl. Acad. Sci.*, doi:10.1073/pnas.0611338104.

Nijssen, B., et al. (2003), Simulation of high latitude hydrological processes in the Torne-Kalix basin: PILPS phase 2 (e) - 2: Comparison of model results with observations, *Global Planet. Change*, *38*, 31–53.

Niu, G. Y., Z. L. Yang, R. E. Dickinson, and L. E. Gulden (2005), A simple TOPMODEL-based runoff parameterization (SIMTOP) for use in global climate models, *J. Geophys. Res.*, *110*, D21106, doi:10.1029/2005JD006111.

Niu, G. Y., Z. L. Yang, R. E. Dickinson, L. E. Gulden, and H. Su (2007), Development of a simple groundwater model for use in climate models and evaluation with Gravity Recovery and Climate Experiment data, *J. Geophys. Res.*, *112*, D07103, doi:10.1029/2006JD007522.

Oleson, K. W., et al. (2004), Technical description of the community land model, *NCAR Tech. Note TN-461+STR*, Natl. Cent. for Atmos. Res., Boulder, Colo.

Oleson, K. W., et al. (2007), CLM3.5 documentation, technical report, Natl. Cent. for Atmos. Res., Boulder, Colo. (Available at http://www.cgd.ucar.edu/tss/clm/distribution/clm3.5/)

Oleson, K. W., et al. (2008), Improvements to the Community Land Model and their impact on the hydrological cycle, *J. Geophys. Res.*, *113*, G01021, doi:10.1029/2007JG000563.

Pielke, R. A., Sr. (2001), Influence of the spatial distribution of vegetation and soils on the prediction of cumulus convective rainfall, *Rev. Geophys.*, *39*(2), 151–177.

Pitman, A. J., et al. (1999), Key results and implications from phase 1(c) of the Project for Intercomparison of Land-Surface Parametrization schemes, *Clim. Dyn.*, *15*, 673–684.

Reichstein, M., et al. (2002), Severe drought effects on ecosystem CO_2 and H_2O fluxes at three Mediterranean evergreen sites: revision of current hypotheses?, *Global Change Biol.*, *8*(10), 999–1017.

Reichstein, M., et al. (2003), Inverse modeling of seasonal drought effects on canopy CO_2/H_2O exchange in three Mediterranean ecosystems, *J. Geophys. Res.*, *108*(D23), 4726, doi:10.1029/2003JD003430.

Richardson, A. D., et al. (2006), A multi-site analysis of random error in tower-based measurements of carbon and energy fluxes, *Agric. For. Meteorol.*, *136*(1–2), 1–18.

Running, S. W., D. D. Baldocchi, D. P. Turner, S. T. Gower, P. S. Bakwin, and K. A. Hibbard (1999), A global terrestrial monitoring network integrating tower fluxes, flask sampling, ecosystem modeling and EOS satellite data, *Remote Sens. Environ.*, *70*, 108–127.

Schär, C., P. L. Vidale, D. Luthi, C. Frei, C. Häberli, M. A. Liniger, and C. Appenzeller (2004), The role of increasing temperature variability in european summer heatwaves, *Nature*, *427*(22), 332–336.

Schmid, H. P. (2002), Footprint modeling for vegetation atmosphere exchange studies: a review and perspective, *Agric. For. Meteorol.*, *113*, 159–183.

Schmid, H. P., C. S. B. Grimmond, F. Cropley, B. Offerle, and H.-B. Su (2000), Measurements of CO_2 and energy fluxes over a mixed hardwood forest in the mid-western United States, *Agric. For. Meteorol.*, *103*, 357–374.

Schmid, H. P., H. B. Su, C. S. Vogel, and P. S. Curtis (2003), Ecosystem-atmosphere exchange of carbon dioxide over a mixed hardwood forest in northern lower Michigan, *J. Geophys. Res.*, *108*(D14), 4417, doi:10.1029/2002JD003011.

Sellers, P. J., M. D. Heiser, and F. G. Hall (1992), Relations between surface conductance and spectral vegetation indexes at intermediate (100 m^2 to 15 km^2) length scales, *J. Geophys. Res.*, *97*(D17), 19,033–19,059.

Sellers, P. J., D. A. Randall, G. J. Collatz, J. A. Berry, C. B. Field, D. A. Dazlich, C. Zhang, G. D. Collelo, and L. Bounoua (1996), A revised land surface parameterization (SiB2) for atmospheric GCMs .1. Model formulation, *J. Clim.*, *9*, 676–705.

Sellers, P. J., et al. (1997), Modeling the exchanges of energy, water, and carbon between continents and the atmosphere, *Science*, *275*(5299), 502–509.

Seneviratne, S. I. and R. Stöckli (2007), The role of land-atmosphere interactions for climate variability in europe, in *Climate Variability and Extremes During the Past 100 Years, Advances in Global Change Research*, vol. 33, edited by S. Brönnimann et al., 390 pp., Springer, New York.

Seneviratne, S. I., D. Luthi, M. Litschi, and C. Schar (2006), Land-atmosphere coupling and climate change in europe, *Nature*, *443*(7108), 205–209.

Sivapalan, M., K. Beven, and E. F. Wood (1987), On hydrologic similarity .2. a scaled model of storm runoff production, *Water Resour. Res.*, *23*(12), 2266–2278.

Stöckli, R., and P. L. Vidale (2004), European plant phenology and climate as seen in a 20-year AVHRR land-surface parameter data set, *Int. J. Remote Sens.*, *25*(17), 3303–3330.

Stöckli, R., and P. L. Vidale (2005), Modeling diurnal to seasonal water and heat exchanges at European FLUXNET sites, *Theor. Appl. Climatol.*, *80*, 229–243.

Stöckli, R., P. L. Vidale, A. Boone, and C. Schär (2007), Impact of scale and aggregation on the terrestrial water exchange: integrating land surface models and rhone catchment observations., *J. Hydrometeorol.*, *8*(5), 1002–1015.

Suni, T., J. Rinne, A. Reissell, N. Altimir, P. Keronen, U. Rannik, M. D. Maso, M. Kulmala, and T. Vesala (2003), Long-term measurements of surface fluxes above a Scots pine forest in Hyytiala, southern Finland, 1996–2001, *Boreal Environ. Res.*, *8*(4), 287–301.

Taylor, K. E. (2001), Summarizing multiple aspects of model performance in a single diagram, *J. Geophys. Res.*, *106*(D7), 7183–7192.

Thornton, P. E., and N. E. Zimmermann (2007), An improved canopy integration scheme for a land surface model with prognostic canopy structure, *J. Clim.*, *20*, 3902–3923.

Thornton, P. E., J.-F. Lamarque, N. A. Rosenbloom, and N. Mahowald (2007), Influence of carbon-nitrogen cycle coupling on land model response to CO_2

fertilization and climate variability, *Global Biogeochem. Cycles*, *21*, GB4018, doi:10.1029/2006GB002868.

Turner, D. P., S. V. Ollinger, and J. S. Kimball (2004), Integrating remote sensing and ecosystem process models for landscape- to regional-scale analysis of the carbon cycle, *Bioscience*, *54*, 573–584.

Urbanski, S., et al. (2007), Factors controlling CO_2 exchange on timescales from hourly to decadal at Harvard forest, *J. Geophys. Res.*, *112*, G02020, doi:10.1029/2006JG000293.

Valentini, R. (Ed.) (2003), *Fluxes of Carbon, Water and Energy of European Forests*, *Ecol. Stud. Ser.*, vol. 163, 274 pp., Springer, New York.

Vidale, P. L., and R. Stöckli (2005), Prognostic canopy air space solutions for land surface exchanges, *Theor. Appl. Climatol.*, *80*, 245–257.

Wilson, K., et al. (2002), Energy balance closure at FLUXNET sites, *Agric. For. Meteorol.*, *113*, 223–243.

Zaitchik, B. F., A. K. Macaldy, L. R. Bonneau, and R. B. Smith (2006), Europe's 2003 heat wave: a satellite view of impacts and land atmosphere feedbacks, *Int. J. Climatol.*, *26*(6), 743–769.

G. B. Bonan, D. M. Lawrence, K. W. Oleson, and P. E. Thornton, Terrestrial Sciences Section, National Center for Atmospheric Research, Boulder, CO 80305, USA.

A. S. Denning, Department of Atmospheric Science, Colorado State University, Fort Collins, CO 80523, USA.

G.-Y. Niu and Z.-L. Yang, Department of Geological Sciences, University of Texas at Austin, Austin, TX 78712, USA.

S. W. Running, Numerical Terradynamics Simulation Group, University of Montana, Missoula, MT 59812, USA.

R. Stöckli, Climate Services, Federal Office of Meteorology and Climatology MeteoSwiss, Krähbühlstrasse 58, 8044 Zürich, Switzerland. (reto.stoeckli@meteoswiss.ch)